Manuscript draft

Title: Novel multitarget inhibitors with antiangiogenic and immunomodulator properties

Article type: Original paper

Keywords: angiogenesis, VEGFR-2, immunotherapy, PD-L1, ureas, docking.

Abstract:

By means of docking studies, seventeen compounds **T.1**-**T17** have been designed and evaluated as multitarget inhibitors of VEGFR-2 and PD-L1 proteins in order to overcome resistance phenomena offered by cancer. All these designed molecules display a urea moiety as a common structural feature and eight of them (**T.1**-**T8**) further contain a 1,2,3-triazol moiety. The antiproliferative activity of these molecules on several tumor cell lines (HT-29, MCF-7, HeLa, A549, HL-60), on the endothelial cell line HMEC-1 and on the non-tumor cell line HEK-293 has been determined. The urea derivatives were also evaluated for their antiangiogenic properties, whereby their ability to inhibit tubulogenesis and kinase activity employing flow cytometry, ELISA, immunofluorescence and western blot techniques was measured. In addition, these techniques were also employed to investigate the immunomodulator action of the synthetic compounds on the inhibition of PD-L1 and c-Myc proteins. Compound **T.2,** 1-(3-chlorophenyl)-3-(2-(4-(4-methoxybenzyl)-1*H*-1,2,3-triazol-1-yl)ethyl)urea, has shown similar results to sorafenib in both down-regulation of VEGFR-2 and inhibition of the kinase activity of this receptor. Furthermore, compound **T.14**, (*E*)-1-(4-chlorophenyl)-3-(3-(4-methoxystyryl)phenyl)urea, improves the effect of **T.2** as regards tube formation of endothelial cells and inhibition of VEGFR-2 tyrosine kinase activity. In addition, **T.14** improves the effect of the experimental drug BMS-8 in the inhibition of PD-L1 and c-Myc proteins.

Novel multitarget inhibitors with antiangiogenic and immunomodulator properties

Laura Conesa-Milián,[a] Eva Falomir,[a] Juan Murga,[a]* Miguel Carda,[a] J. Alberto Marco[b]*

[a]Depart. de Q. Inorgánica y Orgánica, Univ. Jaume I, E-12071 Castellón, Spain

[b]Depart. de Q. Orgánica, Univ. de Valencia, E-46100 Burjassot, Valencia, Spain

*Corresponding authors: efalomir@uji.es, jmurga@uji.es.

ABSTRACT

By means of docking studies, seventeen compounds **T.1**-**T17** have been designed and evaluated as multitarget inhibitors of VEGFR-2 and PD-L1 proteins in order to overcome resistance phenomena offered by cancer. All these designed molecules display a urea moiety as a common structural feature and eight of them (**T.1**-**T8**) further contain a 1,2,3-triazol moiety. The antiproliferative activity of these molecules on several tumor cell lines (HT-29, MCF-7, HeLa, A549, HL-60), on the endothelial cell line HMEC-1 and on the non-tumor cell line HEK-293 has been determined. The urea derivatives were also evaluated for their antiangiogenic properties, whereby their ability to inhibit tubulogenesis and kinase activity employing flow cytometry, ELISA, immunofluorescence and western blot techniques was measured. In addition, these techniques were also employed to investigate the immunomodulator action of the synthetic compounds on the inhibition of PD-L1 and c-Myc proteins. Compound **T.2,** 1-(3-chlorophenyl)-3-(2-(4-(4-methoxybenzyl)-1*H*-1,2,3-triazol-1-yl)ethyl)urea, has shown similar results to sorafenib in both down-regulation of VEGFR-2 and inhibition of the kinase activity of this receptor. Furthermore, compound **T.14**, (*E*)-1-(4-chlorophenyl)-3-(3-(4-methoxystyryl)phenyl)urea, improves the effect of **T.2** as regards tube formation of endothelial cells and inhibition of VEGFR-2 tyrosine kinase activity. In addition, **T.14** improves the effect of the experimental drug BMS-8 in the inhibition of PD-L1 and c-Myc proteins.

KEYWORDS

Angiogenesis, VEGFR-2, immunotherapy, PD-L1, ureas, docking.

1. Introduction

Cancer is a complex pathological process that encompasses a large group of diseases. There is a need therefore to find new drugs able to interfere with most of these processes in order to increase treatment options and to avoid resistance mechanisms.[1] The goal of the present work is the design, synthesis and biological evaluation of molecules with anticancer activity deemed to address two different biological targets of particular relevance in the cancer process. These targets are the tyrosin kinase VEGFR-2 (Vascular Endothelial Growth Factor Receptor 2) and the PD-L1 protein (Programmed Death-Ligand 1).

The first target is related to the angiogenesis process, the growth of new blood vessels from pre-existing vasculature, which is a critical step in tumor progression.[2] Vascular endothelial growth factors (VEGFs) regulate angiogenesis by binding to their associated receptors. Therapeutic inhibition of VEGFR-2 action is now having an impact in the clinical use for the treatment of a number of diseases.[3] The second target is related to the immunosuppressive ability of tumor cells. These overexpress negative immunologic regulators and generate a protected environment. The PD-L1 protein, which is overexpressed in cancer cells, plays a key role in the deregulation of the immune system through formation of PD-1/PD-L1 complex.[4] The present research intends to design compounds with the ability to bind to PD-L1 present in tumor cells, therefore blocking their ability to evade the immune system. Antibodies targeting the PD-1/PD-L1 immune checkpoint have achieved outstanding success in recent years. Clinically available examples include nivolumab and pidilizumab. However, their high immunogenicity and low stability have led to the research for new non-peptidic molecules.[5]

It has been reported that the c-Myc oncogene has a direct role in preventing immune cells from efficiently attacking tumor cells. Indeed, c-Myc fosters tumor growth by increasing the levels of two immune checkpoint proteins, CD47 and PD-L1, which help thwart the host immune response.[6] Thus, c-Myc inactivation in tumors appears to engage the immune system to elicit cellular senescence in tumor cells and to collapse the vascular endothelial cells.[7]

Sorafenib (Figure 1) is an inhibitor of the kinase domain of VEGFR-2. It bears a N,N´-diarylurea fragment that has shown, both through X-ray diffraction studies [8] and through computational studies [9], to be determinant in its interaction with the kinase

domain. Docking studies have revealed that sorafenib can form 5 hydrogen bonds with the kinase domain of VEGFR-2: two with Glu885, two weak links with Cys919 and one with Asp1046. The other interactions with the kinase domain are of the hydrophobic type with the pocket formed by the amino acids Leu840, Val848, Ala866, Ile888, Leu889, Val899, Phe918, Thr916 and Leu1035. It has also been established that the strongest link is formed with the Asp1046.

Brystol-Myers Squibb reported in 2015 the discovery of the first non-peptidic molecules able to inhibit the formation of the PD-1/PD-L1 complex [10]. The mode of interaction of these compounds, indicated as BMS-8, BMS-37, BMS-202 and BMS-242 in Figure 1, was established in 2016 [11]. Using differential scanning fluorimetry (DSF) techniques, it was determined that these compounds induce thermal stabilization of PD-L1. Finally, the protein bound to the substrates was crystallized and the binding sites determined. Thus, these compounds are linked in a hydrophobic groove formed by the amino acids Tyr56, Met115, Ile116, Ala121 and Tyr123 and promote the dimerization of PD-L1 protein. Thus, it is possible to inhibit the formation of the PD-1/PD-L1 complex by means of a double pathway: the inhibitors occupy part of the area involved in the PD-1/PD-L1 interaction and, in addition, when the dimer is formed between two PD-L1 molecules, one of them has the opposite orientation to the one necessary to interact with PD-1. Consequently, the interaction between PD-1 and PD-L1 is disabled.

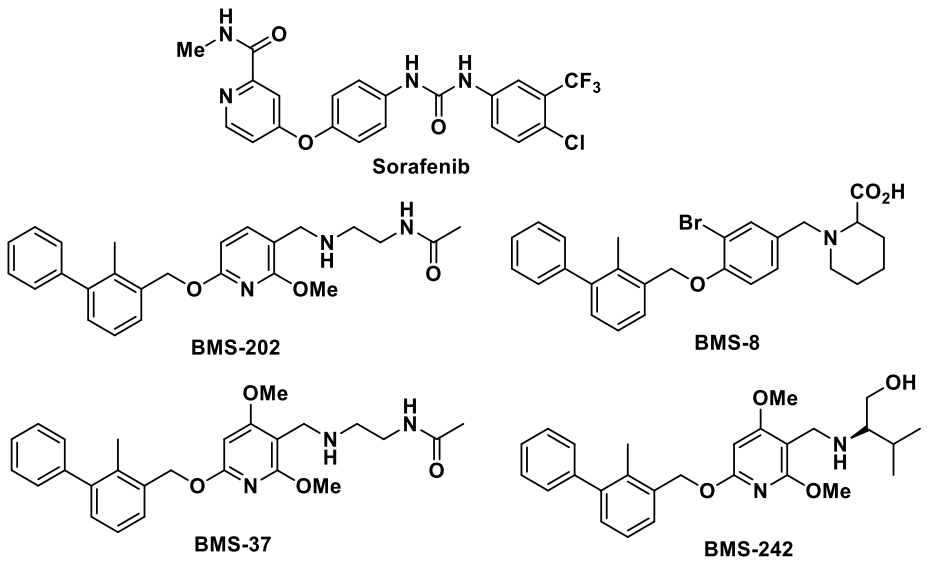

Figure 1. Structure of sorafenib and non-peptidic inhibitors of PD-L1.

Both the binding site of sorafenib in the kinase domain of VEGFR-2 and the binding site in PD-L1 possess a hydrophobic groove in which aromatic rings can be inserted. Our

goal is the design of compounds able to interact with both binding sites and act as multitarget inhibitors.

2. Results and discussions

2.1. Preliminary docking study

We have carried out a docking study using AutoDock 4.2 software [12] on the kinase domain of VEGFR-2 and on the site identified in PD-L1 in order to locate relatively simple structures that are able to interact with both sites. Several general structures capable of establishing at least three of the hydrogen bonds shown by sorafenib (see Figure 2) and of interacting with the binding site in PD-L1 have been identified by us. These structures are characterized by having a urea system (which is essential to allow its interaction with the kinase domain) to which aromatic rings are bound in order to interact with the hydrophobic grooves present in both proteins.

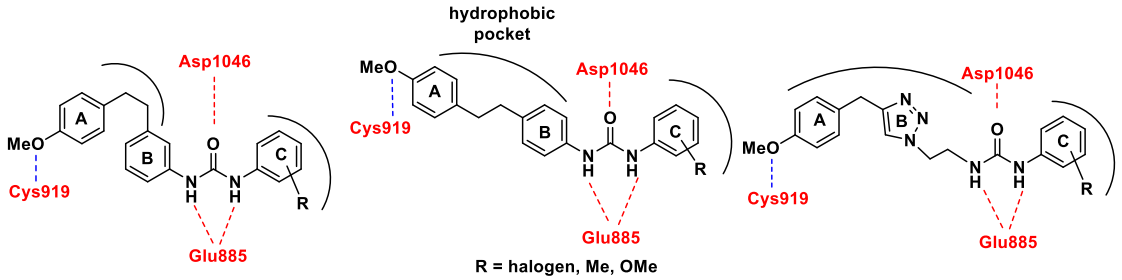

Figure 2. Identified general structures able to interact with the kinase domain of VEGFR-2 and PD-L1. The hydrogen bonds that can be formed with VEGFR-2 are indicated in red. The zones of the molecules that interact with the hydrophobic pockets of both binding sites are also indicated.

As an example, the docking obtained for three of the analyzed structures is shown in Figure 3. It can be appreciated in Figure 3A that compounds **D.1**, **D.2** and **D.3** occupy the binding site in the kinase domain of VEGFR-2 in much the same way as sorafenib does. These compounds establish hydrogen bonds between the OMe group and Cys919, between the two NH groups of the urea system and Glu885 and between the O of urea and Asp1046. The three aromatic rings interact with two hydrophobic zones present in the binding site. It can be seen in Figure 3B that structures **D.1**, **D.2** and **D.3** also occupy the binding site of BMS-202 in PD-L1 protein. The aromatic rings are inserted in a hydrophobic groove with the A rings establishing interactions with Tyr56, Me115 and Ala121, whereas ring B interacts with Tyr123. The more polar urea system points towards the outer zone of the groove.

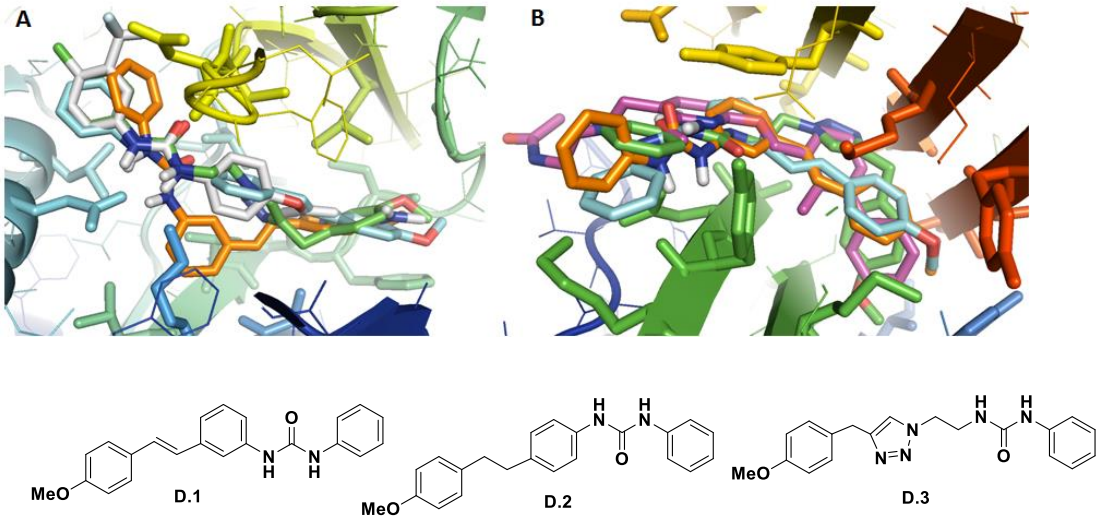

Figure 3. A) Superposition of **D.1** (orange), **D.2** (light blue), **D.3** (green) and sorafenib (grey) in the kinase domain of VEGFR-2. B). Superposition of **D.1** (orange), **D.2** (light blue), **D.3** (green) and BMS-202 (violet) at the PD-L1 binding site.

With the objective to verify these preliminary results obtained from the in-silico study, we envisaged the synthesis and the biological evaluation of several compounds derived from the general structures **D.4**-**D.7** shown in Figure 4. Additionally, differential scanning fluorometry and free protein detection by ELISA were performed prior to the development of the corresponding cellular assays in order to verify the interaction between the targets of study and the designed compounds (see Supporting Information S2 and S3).

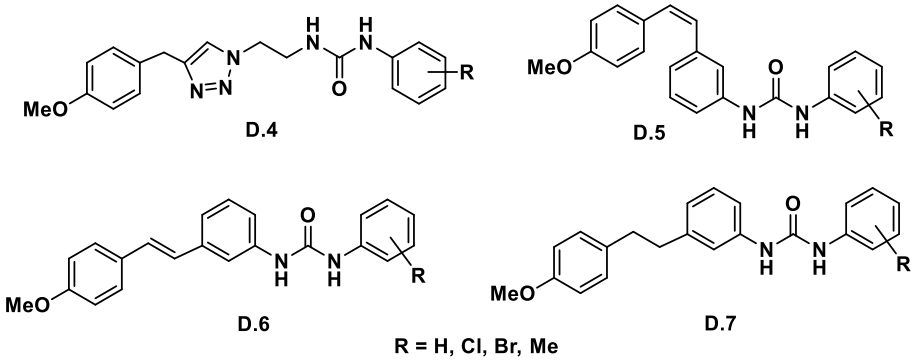

Figure 4. Potential multitarget inhibitors of VEFGR-2 and PD-L1.

2.2.Synthetic work of triazolyl-ureas T.1-T.8

To begin with, we decided to synthesize triazoles with the general structure **D.4** due to its easy synthetic accessibility. These compounds were obtained in only two synthetic steps from 2-azidoethan-1-amine **1** as indicated in Scheme 1 [13]. Thus, treatment of azidoamine **1** with carbonyl diimidazole in the presence of triethylamine generated the

corresponding imidazolide which was then allowed to react with a range of anilines to afford azido-ureas **2-9**. These were then converted into triazolyl-ureas **T.1-T8** upon copper-catalyzed 1,3-dipolar cycloaddition [14] with 1-methoxy-4-(prop-2-yn-1-yl)benzene (for the preparation of this compound see the Experimental section).

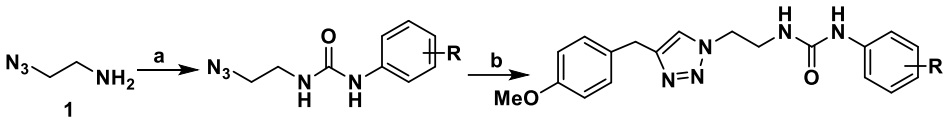

2 (R = H)
3 (R = *m*-Cl)
4 (R = *p*-Cl)
5 (R = *m*-Br)
6 (R = *p*-Br)
7 (R = *o*-Me)
8 (R = *m*-Me)
9 (R = *p*-Me)

T.1 (R = H)
T.2 (R = *m*-Cl)
T.3 (R = *p*-Cl)
T.4 (R = *m*-Br)
T.5 (R = *p*-Br)
T.6 (R = *o*-Me)
T.7 (R = *m*-Me)
T.8 (R = *p*-Me)

Scheme 1

Reagents and conditions: (a) CDI, Et_3N, DMF, 3 h, rt, then the appropriate aniline, 50ºC, overnight; (b) 1-methoxy-4-(prop-2-yn-1-yl)benzene, $CuSO_4 \cdot 5H_2O$, sodium ascorbate, DMF/H_2O (9/1), 60ºC, 2 h.

Unfortunately, all attempts to prepare the *ortho*-halogenated isomers failed due probably to the steric hindrance caused by the halogen in *ortho* position.

2.3.Biological evaluation of triazolyl-ureas T.1-T.8

2.3.1. Cell proliferation inhibition

The ability of triazolyl-ureas **T.1**-**T.8** to inhibit cell proliferation was established by means of their IC_{50} values towards the human tumor cell lines HT-29 (colon adenocarcinoma), MCF-7 (breast adenocarcinoma), HeLa (epithelioid cervix carcinoma) and A549 (pulmonary adenocarcinoma), as well as towards the endothelial cell line HMEC-1 (human microvascular endothelial cells) and the non-tumor cell line HEK-293 (human embryonic kidney cells). All the IC_{50} values observed were higher than 200 μM in all the cell lines tested and are not listed here.

2.3.2. Effect on cellular VEGFR-2

The effect of compounds **T.1**-**T.8** on VEGFR-2 in HMEC-1 cell line was determined by flow cytometry technique. For this assay, cells were incubated for 24 hours in the presence of the corresponding compounds at 100 μM concentration. Then, cells were fixed with formaldehyde and treated with anti-VEGFR-2-alexafluor®647 to quantify membrane VEGFR-2 by flow cytometry. On the other hand, permeabilization of cells

with Triton X-100 prior to fixation step, allowed the quantification of total VEGFR-2 in cells. Table 1 shows the effect of the selected derivatives on VEGFR-2 expression and distribution in HMEC-1 endothelial cell line, referred to control (DMSO, 100%).

Table 1. Effect on VEGFR-2 in HMEC-1 cells.

Comp.	Membrane VEGFR-2 (%)	Total VEGFR-2 (%)
Sorafenib	46 ± 8	64 ± 4
T.1	97 ± 14	105 ± 10
T.2	74 ± 6	81 ± 14
T.3	90 ± 4	102 ± 5
T.4	79 ± 10	78 ± 1
T.5	40 ± 10	55 ± 5
T.6	79 ± 9	100 ± 11
T.7	76 ± 4	91 ± 9
T.8	97 ± 15	90 ± 7

Data are the average (±SD) of three experiments.

Results from Table 1 indicate that compound **T.5** (*p*-Br) is the derivative that shows the strongest interaction with VEGFR-2 in HMEC-1 cells, improving the effect exerted by sorafenib. Some of the other compounds (**T.2**, **T.4**, **T.6**, **T.7**) were also able to down-regulate the expression of VEGFR-2 but to a lesser extent.

Table 2 depicts the effect of **T.2**, **T.4** and **T.5** on VEGFR-2 expression and distribution in A549 tumor cell line at 100 μM concentration, referred to control (DMSO, 100%).

Table 2. Effect on VEGFR-2 in A549 cells.

Comp.	Membrane VEGFR-2 (%)	Total VEGFR-2 (%)
Sorafenib	92 ± 3	85 ± 5
Sunitinib	66 ± 8	135 ± 14
T.2	95 ± 3	86 ± 6
T.4	98 ± 6	80 ± 8
T.5	70 ± 4	61 ± 11

Data are the average (±SD) of three experiments.

Results from Table 2 indicate again that **T.5** (*p*-Br) is the derivative that shows the strongest interaction with VEGFR-2 in A549 cells improving the effect exerted by the reference compound.

2.3.3. *Inhibition of VEGFR-2 kinase activity*

The interaction VEGF/VEGFR-2 causes phosphorylation of the receptor and triggers the signaling cascade that promotes phosphorylation of Erk1/2 (extracellular signal-regulated kinase) and, subsequently, activation of the angiogenesis process [15].

In view of the fact that triazolyl-ureas **T.1**-**T.8** interact with VEGFR-2 on endothelial cells, their capacity to inhibit kinase activity was also studied. Thus, HMEC-1 cells were treated with the derivatives for 24 h at 100 μM, then the cells were lysed and phospho-VEGFR-2 was quantified by ELISA analysis. Western blot analysis of the compounds that were active in inhibiting phospho-VEGFR-2 allowed the relative quantification of phospho-Erk1/2. Table 3 shows the percentage of p-VEGFR-2 and p-Erk for each compound referred to control (DMSO, 100%).

Table 3. p-VEGFR-2 and p-Erk1/2 detected in HMEC-1 cells.

Comp.	HMEC-1 p-VEGFR-2 (%)	HMEC-1 p-Erk1/2 (%)
Sorafenib	77 ± 9	80 ± 8
T.1	100 ± 12	-
T.2	70 ± 16	38 ± 14
T.3	86 ± 3	72 ± 6
T.4	>100	-
T.5	>100	-
T.6	83 ± 4	82 ± 11
T.7	90 ± 10	-
T.8	>100	-

Data are the average (±SD) of three experiments.

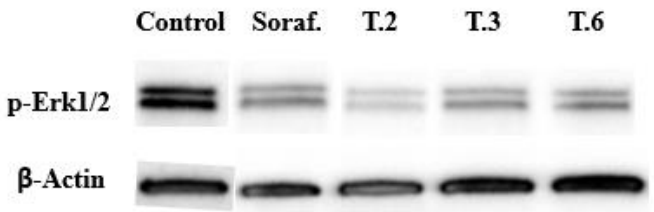

Figure 5. Representative Western blot of p-Erk1/2 detection in HMEC-1 cells. β-actin was used as internal control.

Table 3 shows that the best inhibitory kinase activity in endothelial cells is shown by **T.2** (*m*-chloro), **T.3** (*p*-chloro) and **T.6** (*o*-methyl) which are able to reduce the phosphorylation of VEGFR-2 at levels similar to sorafenib. Interestingly, there is an

important inhibition of Erk1/2 phosphorylation by **T.2**, improving the results obtained with sorafenib.

On the other hand, inhibition of VEGFR-2 kinase activity in A549 cells was also tested but in this case, none of the selected derivatives improved the effect observed for sorafenib. Table 4 shows the percentage of p-VEGFR-2 and p-Erk for each compound referred to control (DMSO, 100%).

Table 4. p-VEGFR-2 and p-Erk1/2 detected in A549 cells.

Comp.	A549 p-VEGFR-2 (%)	A549 p-Erk1/2 (%)
Sorafenib	84 ± 4	50 ± 7
T.2	121 ± 11	99 ± 9
T.3	125 ± 12	78 ± 7
T.6	121 ± 16	119 ± 8
T.7	112 ± 10	90 ± 13

Data are the average (±SD) of three experiments.

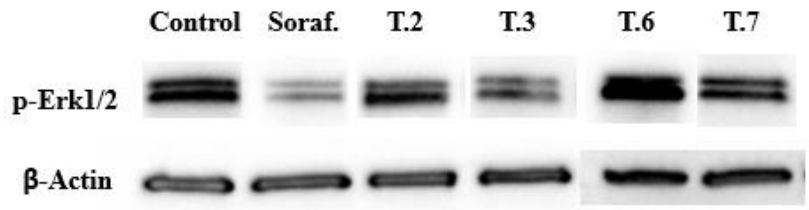

Figure 6. Representative Western blot of p-Erk1/2 detection in A549 cells. β-actin was used as internal control.

2.3.4. Tube formation inhibition on endothelial cells

Antiangiogenic agents mainly affect endothelial cells. Thus, the capacity of synthetic compounds to inhibit the formation of new vasculature network formed by HMEC-1 was evaluated. Therefore, cells were seeded on top of Matrigel® and simultaneously treated with different concentrations of derivatives. Pictures were taken 24 h later in order to evaluate the tube formation inhibition effect. Table 5 shows the minimum concentration at which compounds are active in the tube formation inhibition. Only **T.2**, **T.3** and **T.6** were tested, since they showed the highest activities in the inhibition of VEGFR-2 kinase activity (see Table 3).

Table 5. Inhibition effect of tube formation.

Comp.	Minimum active conc. (μM)
Sunitinib	3
Sorafenib	10

T.2	50
T.3	400
T.6	200

Data are representative of three experiments.

Data from Table 5 confirm that triazolyl-ureas are able to inhibit tube formation but at higher doses than sunitinib and sorafenib, with **T.2** (*m*-chloro) being the most potent compound.

2.3.5. Effect on PD-L1 and c-Myc proteins

In order to evaluate the immunomodulator properties of the synthetic derivatives, the effect on PD-L1 and c-Myc proteins by the selected compounds was studied. Thus, compounds were added to A549 cells at 100 μM concentration and, after 24 h, cells were lysed and ELISA analysis was performed to determine the relative amount of both proteins compared to DMSO treated cells. Table 6 shows the percentage of free PD-L1 detected for each compound referred to control (DMSO). The percentage of c-Myc has been quantified only for the compounds which exerted a similar or better action than the reference compound BMS-8 in the inhibition of PD-L1.

Table 6. PD-L1 and c-Myc detection in A549 cells.

Comp.	% PD-L1	% c-Myc
BMS-8	68 ± 5	60 ± 7
T.1	83 ± 9	-
T.2	70 ± 8	60 ± 8
T.3	69 ± 10	73 ± 5
T.4	80 ± 12	-
T.5	>100	-
T.6	82 ± 20	-
T.7	90 ± 20	-
T.8	66 ± 6	70 ± 8

Data are the average (±SD) of three experiments.

From Table 6 it can be concluded that compounds **T.2** (*m*-chloro), **T.3** (*p*-chloro) and **T.8** (*p*-methyl) inhibit PD-L1 and c-Myc proteins in a similar way to BMS-8.

2.3.6. Cell proliferation evaluation in co-cultures

Some tumor cell lines such as A549 and HT-29 show high PD-L1 overexpression.[16] Therefore, cell proliferation of these has been studied in presence of PD-1 expressing

Jurkat T cells in order to evaluate whether the observed cell proliferation inhibition is due to the blockage of PD-1/PD-L1 system. Compounds which showed good PD-L1 inhibition in ELISA test were evaluated. Thus, tumor cells were treated for 24 h with the selected compounds at 200 µM in presence of Jurkat T cells and then, living cells were counted using trypan blue and a Neubauer chamber. Figure 7 shows the inhibition of tumour cell proliferation exhibited by the derivatives due to the presence of Jurkat T cells.

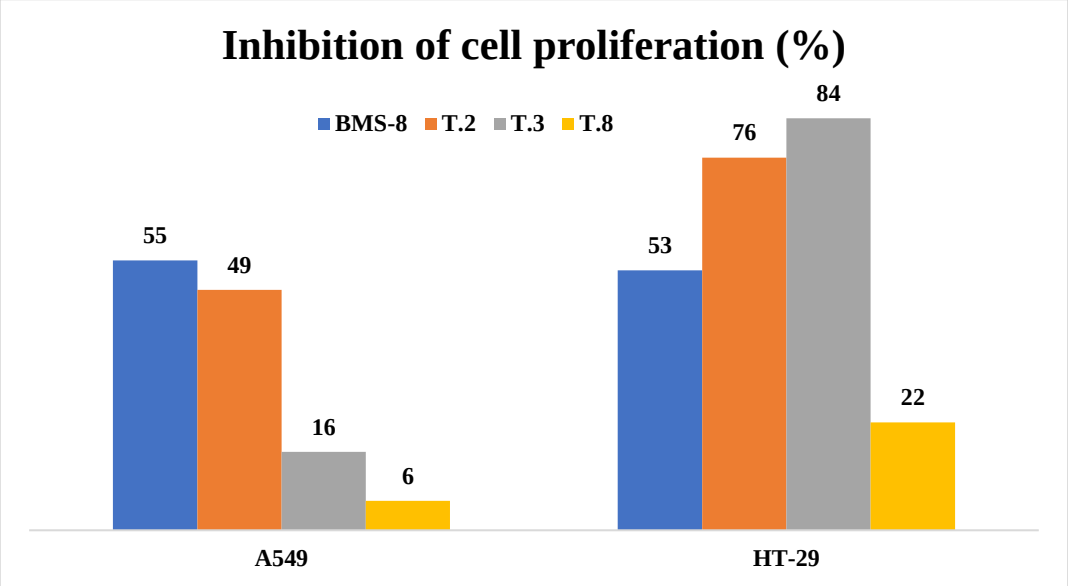

Figure 7. Inhibition of cell proliferation (%) in presence of Jurkat T cells. Data are representative of three experiments.

From data provided in Figure 7, it can be concluded that the tested compounds are able to inhibit A549 cell proliferation in co-culture but do no improve the effect exerted by BMS-8. Interestingly, in the HT-29 cell line this effect is much higher for compounds **T.2** (*m*-chloro) and **T.3** (*p*-chloro), improving the effect exhibited by BMS-8.

2.4. Synthesis of ureas T.9-T.17

The triazolyl-ureas that contain a chlorine atom in their structure are the compounds that display the best activities in our biological tests and these were very similar to the ones exhibited by our reference compounds sorafenib and BMS-8. Therefore, we decided to prepare new compounds with general structures **D.5**-**D.7** (Fig. 4) containing a chlorine atom in the phenyl ring. The synthesis of these compounds is depicted in Scheme 2. Thus, Wittig reaction of phosphonium salt **11** with 4-methoxybenzaldehyde afforded 1-(4-methoxystyryl)-3-nitrobenzene **12** as a mixture of *E/Z* isomers. Reduction of this mixture gave rise to a mixture of *E/Z* anilines which was separated by column chromatography to

afford (*Z*)-3-(4-methoxystyryl)aniline **13** and (*E*)-3-(4-methoxystyryl)aniline **14**. On the other hand, hydrogenation of **12** led to 3-(4-methoxyphenethyl)aniline **15**. Compounds **13**, **14** and **15** were converted into carbamates **16**, **17** and **18** [17], which upon reaction with chloroanilines gave rise to ureas **T.9**-**T.17**.

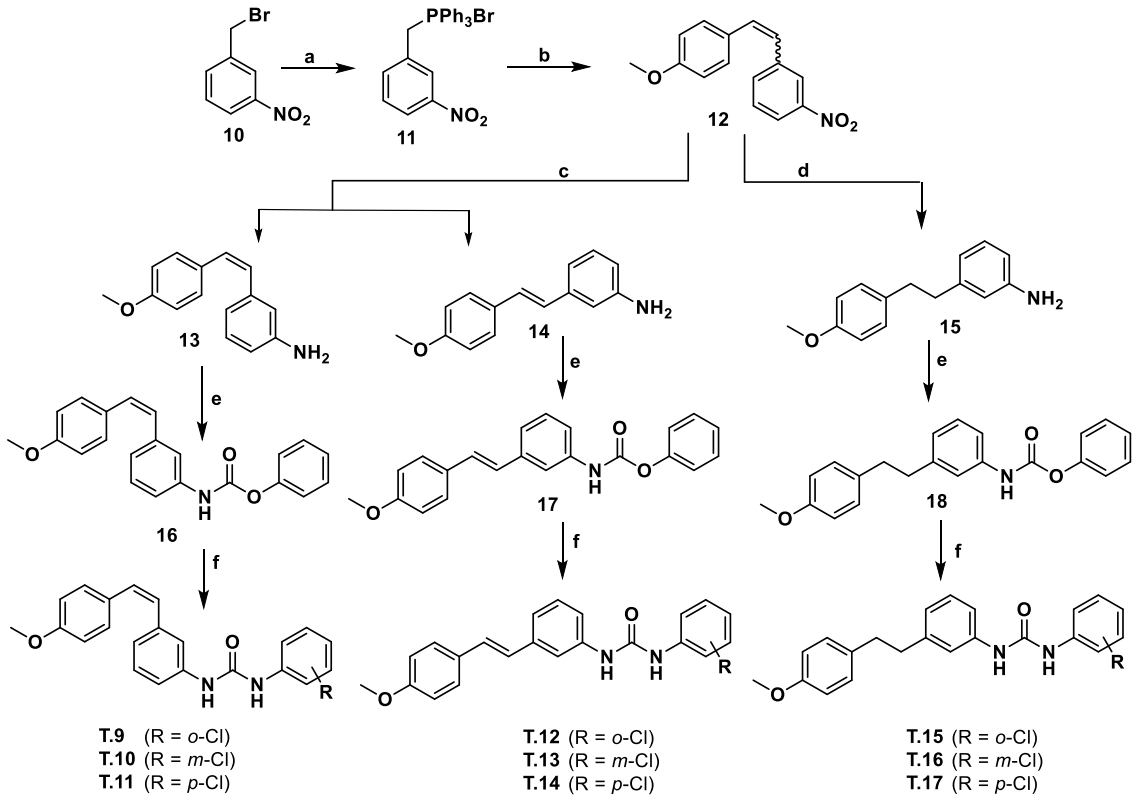

Scheme 2

Reagents and conditions: (a) PPh_3, CH_2Cl_2, 3 h, rt., 71%; (b) 4-methoxybenzaldehyde, K_2CO_3, 18-crown-6, CH_2Cl_2, reflux, overnight, 73%; (c) Zn, AcOH, 1 h, rt., (*Z*/*E* 6:4); (d) H_2, Pd/C, EtOAc, 2 h, rt., 66%; (e) phenyl chloroformate, pyridine, THF, 0ºC 30 min, then 1 h rt.; (f) the appropriate chloroaniline, Et_3N, THF, 40-50ºC.

2.5. Biological evaluation of ureas T.9-T.17

2.5.1. Cell proliferation inhibition

The ability of ureas **T.9**-**T.17** to inhibit cell proliferation was established by means of their IC_{50} values towards the human tumor cell lines HT-29 (colon adenocarcinoma), MCF-7 (breast adenocarcinoma), HeLa (epithelioid cervix carcinoma) and A549 (pulmonary adenocarcinoma), as well as towards the endothelial cell line HMEC-1 (human microvascular endothelial cells) and the non-tumor cell line HEK-293 (human embryonic kidney cells). The IC_{50} values for ureas **T.9**-**T.17** are presented in Table 7 along with IC_{50} values for the reference compounds sunitinib, sorafenib and BMS-8.

Table 7. IC_{50} values (μM) for sunitinib, sorafenib, BMS-8 and derivatives **T.9**-**T.17**.[a]

Comp.	HT-29	MCF-7	HeLa	A549	HMEC-1	HEK-293
Sunitinib	3.8 ± 0.5	0.08 ± 0.02	7.8 ± 1.0	11 ± 2	7 ± 4	5.0 ± 0.8
Sorafenib	17 ± 4	14 ± 4	6.1 ± 0.4	27 ± 2	34 ± 3	5.0 ± 0.7
BMS-8	19 ± 2	20 ± 3	>100	6 ± 1	-	60 ± 10
T.9	12 ± 4	19 ± 2	22 ± 3	21 ± 9	33.0 ± 0.6	6.5 ± 0.2
T.10	20 ± 10	37.2 ± 0.8	10.5 ± 0.6	38 ± 3	32.9 ± 0.5	5 ± 2
T.11	33 ± 5	17 ± 3	8 ± 1	29 ± 3	33 ± 3	20 ± 10
T.12	47 ± 4	>100	>100	61 ± 3	>100	57 ± 3
T.13	3.5 ± 0.6	4.3 ± 0.7	11.3 ± 0.7	7.7 ± 0.2	2 ± 1	2.4 ± 0.6
T.14	0.52 ± 0.09	0.40 ± 0.09	0.7 ± 0.3	1.5 ± 0.9	1.8 ± 0.8	1.0 ± 0.4
T.15	20 ± 3	>100	69 ± 5	24 ± 5	48 ± 7	90 ± 10
T.16	14 ± 4	8.2 ± 0.6	16.5 ± 0.7	>200	50 ± 20	5.3 ± 0.9
T.17	1.5 ± 0.1	15.3 ± 0.4	21 ± 1	>200	>200	1.8 ± 0.7

[a]IC_{50} values are expressed as the compound concentration that inhibits the cell growth by 50%. Data are the average (±SD) of three experiments.

The synthetic ureas show antiproliferative activity in the low micromolar range in all tested cell lines, comparable to that shown by reference compounds sunitinib, sorafenib and BMS-8. The (*E*)-*p*-chloro derivative **T.14** was the most active one with IC_{50} values at submicromolar level, and exhibited lower IC_{50} values in cancer cell lines than in non-tumour endothelial ones. This fact allowed us to study the biological activity of this compound at a concentration that does not affect non-tumour cell lines.

2.5.2. Induction of apoptosis

Apoptosis represents a universal and exquisitely efficient cellular suicide pathway [18]. This phenomenon can be triggered by intrinsic signals such as genotoxic stress, or extrinsic signals such as the binding of ligands to cell surface death receptors [19]. Induction of apoptosis was studied by measuring the translocation of phosphatidylserine from the cytoplasmic to the extracellular side of the plasma membrane. Thus, A549 cells were incubated for 24 h in the presence of compounds at 100 μM, after which annexin-V binding was measured by flow cytometry. The apoptotic effect of compounds **T.9**-**T.17** is indicated in Figure 8.

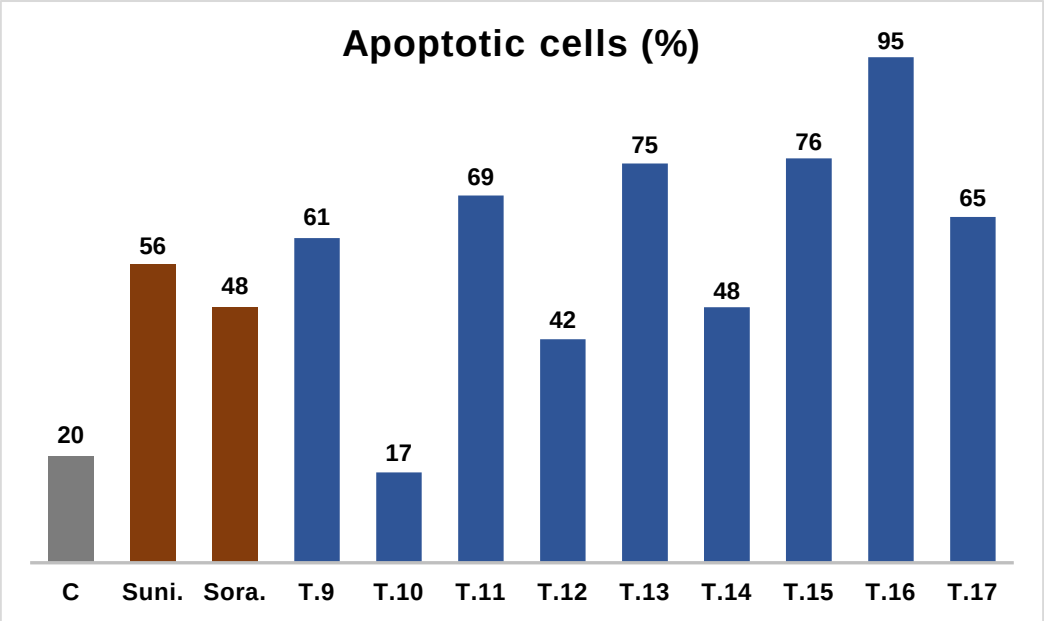

Figure 8. Apoptotic effect (%) in A549 cells. Data are representative of three experiments.

All the tested compounds induce apoptosis at 100 μM, with the exception of compound **T.10**, which exhibited an activity similar to that of control (DMSO). Moreover, compounds **T.11, T.13, T.15, T.16** and **T.17** improve the effect depicted by sunitinib and sorafenib. BMS-8 and **T.1-T.8** derivatives were also tested but they did not exhibit any effect in the induction of apoptosis.

2.5.3. Effect on cellular VEGFR-2

The effect of ureas **T.9-T.17** on VEGFR-2 in A549 tumor cell line was determined by both flow cytometry and immunofluorescence techniques. For these assays, cells were incubated for 24 hours in the presence of the corresponding compounds at 10 μM concentration. Table 8 and Figure 7 show the results obtained for each compound on free VEGFR-2 presence and distribution in A549 cell line, referred to control (DMSO).

Table 8. Effect on VEGFR-2 expression in A549 cells.

Comp.	Membrane VEGFR-2 (%)	Total VEGFR-2 (%)
Sorafenib	92 ± 3	85 ± 5
Sunitinib	66 ± 8	135 ± 14
T.9	114 ± 20	177 ± 9
T.10	102 ± 10	186 ± 10
T.11	118 ± 3	100 ± 7
T.12	109 ± 18	42 ± 9

T.13	52 ± 10	32 ± 4
T.14	56 ± 11	10 ± 2
T.15	100 ± 19	100 ± 16
T.16	97 ± 10	98 ± 3
T.17	97 ± 11	96 ± 7

Data are the average (±SD) of three experiments.

(E) derivatives **T.13** (*m*-chloro) and **T.14** (*p*-chloro) were the best ones in reducing the presence of VEGFR-2, therefore improving the effect exerted by sorafenib. Indeed, they were able to down-regulate VEGFR-2 to the half of the control inhibiting internalization of the target and reducing the total level of the protein to 10-30 % of the control.

Immunofluorescence assay correlated well with flow cytometry results. Figure 9 shows that both compounds **T.13** (B) and **T.14** (C) caused a significant reduction of membrane VEGFR-2 and compound **T.14** exerted a higher inhibition of the internalization of the protein to the nucleus.

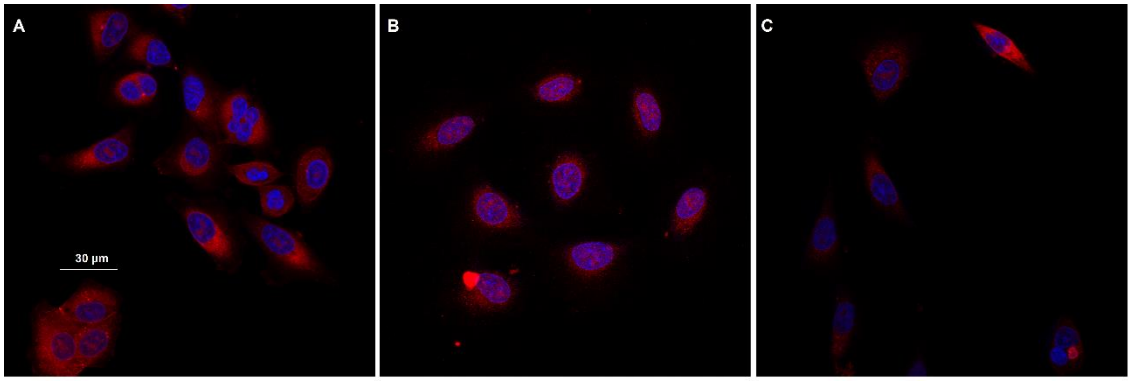

Figure 9. Effect on VEGFR-2 expression in A549 cells (A) DMSO, (B) **T.13** and (C) **T.14**.

The effect of *(E)* derivatives on VEGFR-2 presence and distribution in endothelial cells was also evaluated (see Table 9), referred to control (DMSO).

Table 9. Effect on VEGFR-2 expression in HMEC-1 cells.

Comp.	Membrane VEGFR-2 (%)	Total VEGFR-2 (%)
Sorafenib	46 ± 8	64 ± 4
T.12	76 ± 9	121 ± 8
T.13	55 ± 8	106 ± 16
T.14	56 ± 8	109 ± 17

Data are the average (±SD) of three experiments.

Results from Table 9 indicate that the *(E)* derivatives did not inhibit internalization of VEGFR-2 in HMEC-1 cells but reduced the presence of the target in the membrane. Again, **T.13** and **T.14** exhibited the highest activities, similar to sorafenib.

2.5.4. *Inhibition of VEGFR-2 kinase activity*

The effect on kinase activity of VEGFR-2 exerted by the *(E)* derivatives was studied by western blot on two cell lines, A549 and HMEC-1. In this case, cells were treated for 24 h at 10 μM concentration of the corresponding compounds. Table 10 shows the relative amount of p-VEGFR-2 and p-Erk1/2 detected on A549 when treated with each compound referred to control (DMSO).

Table 10. p-VEGFR-2 and p-Erk1/2 detected in A549 cells.

Comp.	A549 p-VEGFR-2 (%)	A549 p-Erk1/2 (%)
Sorafenib	84 ± 4	50 ± 7
T.12	76 ± 3	100 ± 18
T.13	75 ± 5	56 ± 12
T.14	82 ± 3	66 ± 8

Data are the average (±SD) of three experiments.

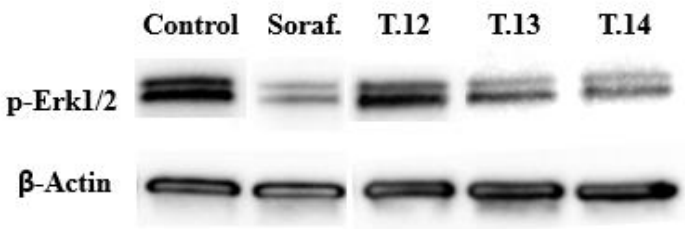

Figure 10. Representative Western blot of p-Erk1/2 detection in A549 cells. β-actin was used as internal control.

Table 10 shows that **T.13** and **T.14** reduce VEGFR-2 and Erk1/2 phosphorylation in the tumor cell line in a similar way to sorafenib. However, no effect on the kinase activity of VEGFR-2 on the endothelial cell line HMEC-1 was observed for any of the tested compounds.

2.5.5. *Tube formation inhibition on endothelial cells*

The capacity of ureas **T.9-T.17** to inhibit the formation of new vasculature network formed by HMEC-1 was evaluated. Table 11 shows the minimum concentration at which compounds are active and begin to inhibit the microtube formation.

Table 11. Inhibition effect of tube formation.

Comp.	Minimum active conc. (μM)
Sunitinib	3
Sorafenib	10
T.9	10
T.10	10
T.11	1
T.12	10
T.13	0.1
T.14	0.1
T.15	1
T.16	10
T.17	100

Data are representative of three experiments.

A comparison of the minimum active concentration values to IC_{50} values for HMEC-1 cell line (see Table 7) shows that there is a correlation between antiproliferative activity and tube formation inhibition capacity, as compounds with lower IC_{50} values exhibit microtube inhibition activity at lower concentrations. Moreover, it is observed that some of the tested compounds are more active than sunitinib and sorafenib, particularly *(E)* derivatives **T.13** (*m*-chloro) and **T.14** (*p*-chloro), which are 100-fold more active than sorafenib. Pictures for the inhibition of neovascularization achieved by compound **T.14**, at different concentrations, are displayed in Figure 11.

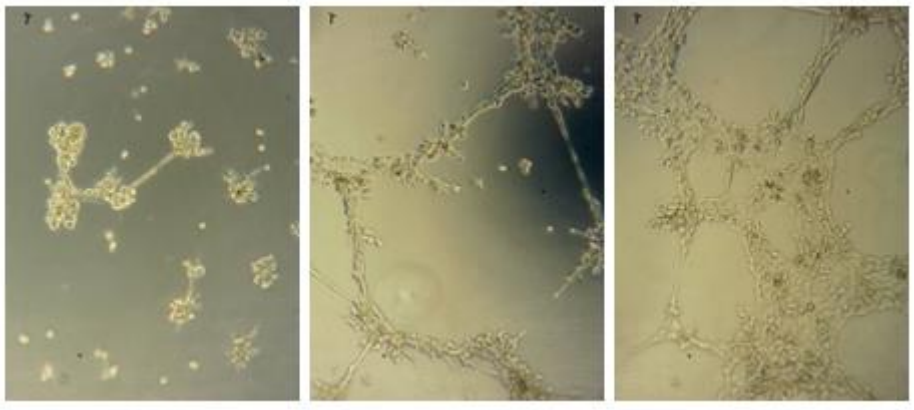

Figure 11. Effect of **T.14** at 1, 0.1 and 0.01 μM concentrations (from left to right).

2.5.6. Effect on PD-L1 and c-Myc proteins

We also evaluated the immunomodulator properties of these derivatives in the same way as described above for the triazole derivatives. Thus, the effect on PD-L1 and c-Myc proteins by the selected compounds was studied by ELISA on A549 cells. After 24 h treatment at 100 μM concentration of compounds, cells were lysed and ELISA analysis was performed to determine the relative amount of both proteins compared to DMSO treated cells. Table 12 shows the percentage of free PD-L1 detected for each compound referred to control (DMSO). Again, the percentage of c-Myc has been quantified only for the compounds which exerted similar or better action than the reference compound BMS-8 in the inhibition of PD-L1.

Table 12. PD-L1 and c-Myc proteins detection in A549 cells.

Comp.[a]	% PD-L1	% c-Myc
BMS-8	68 ± 5	60 ± 7
T.9	83 ± 3	-
T.10	92 ± 10	-
T.11	75 ± 6	-
T.12	74 ± 7	-
T.13	49 ± 8	65 ± 12
T.14	25 ± 9	37 ± 5
T.15	61 ± 6	63 ± 11
T.16	51 ± 9	51 ± 10
T.17	38 ± 3	44 ± 6

[a] **T.9-T.14** were tested at 15 μM. BMS-8 and **T.15-T.17** were tested at 100 μM. Data are the average (±SD) of three experiments.

From Table 12 it can be deduced that compounds **T.13**, **T.14**, **T.16** and **T.17** are able to inhibit PD-L1 and c-Myc proteins and display a stronger effect than that exerted by BMS-8, with **T.14 (***p*-chloro) being the most active in both targets.

Subsequently, immunofluorescence was performed for compound **T.14**. For this assay, cells were incubated for 24 hours at 100 μM of treatment. Then, cells were fixed, permeabilized and treated with anti-PD-L1-alexafluor®647 and anti-c-Myc-FITC. The pictures shown in Figure 12 correlate well with the results obtained by ELISA test (Table 12), since compound **T.14** (C) inhibits PD-L1 and c-Myc proteins in a higher proportion than BMS-8 (B).

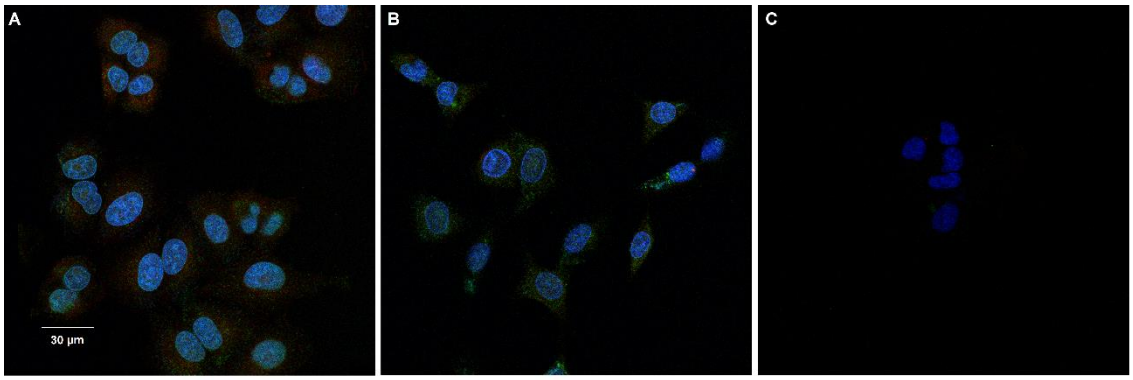

Figure 12. Effect on PD-L1 (red) and c-Myc (green) in A549 cells. (A) DMSO, (B) BMS-8, (C) **T.14**.

2.5.7. *Cell proliferation evaluation in co-cultures*

We also studied the effect of compounds **T.13**, **T.14** and **T.17**, which showed good PD-L1 inhibition, in affecting tumor cell proliferation in the presence of PD-1 expressing Jurkat T-cells. Thus, A549 were treated for 24 h with the selected compounds at 200 µM in presence of Jurkat T cells. Then, living cells were counted using trypan blue and a Neubauer chamber. Figure 13 shows the inhibition of tumor cell proliferation exhibited by **T.13**, **T.14** and **T.17** due to the presence of Jurkat T cells.

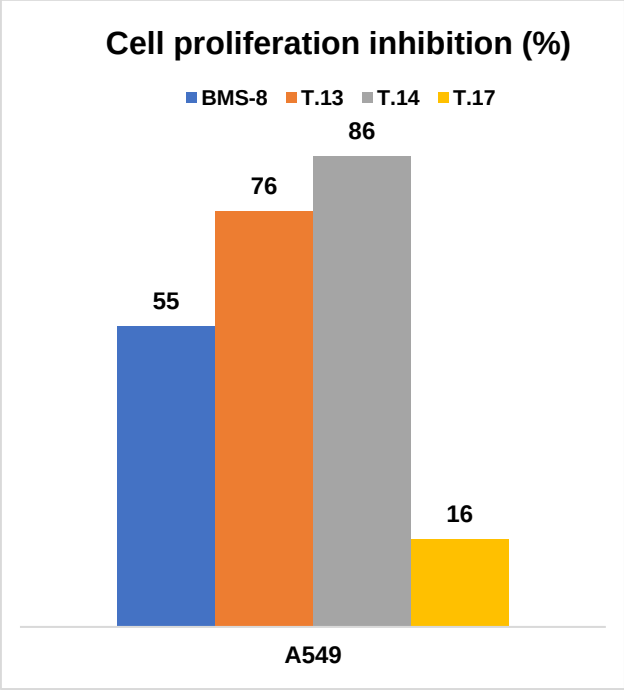

Figure 13. Inhibition of cell proliferation (%) in presence of Jurkat T cells. Data are representative of three experiments.

Data provided in Figure 13 shows that **T.13** and **T.14** were able to inhibit A549 cell proliferation in co-culture improving the effect exerted by BMS-8. Therefore, it can be affirmed that these derivatives act by means of disturbing PD-1/PD-L1 interactions.

3. Summary and conclusions

The biological study of triazolyl ureas **T.1-T.8** has revealed that derivatives with chlorine substitution in *meta* or *para* positions of the benzene ring are the most active as antiangiogenic and immunomodulator agents. Indeed, **T.2** (*m*-Cl) has proven very effective in both down-regulation of VEGFR-2 and inhibition of the kinase activity of this receptor, better results being observed than with the reference compounds. Regarding the immunomodulator properties, **T.2** has been the most effective triazolyl urea in inhibiting cell proliferation in co-cultures, since due to its interaction with PD-L1 it has increased its antiproliferative effect in almost a 50%.

In search of higher activities than those observed with the triazolyl ureas, we synthetized a second group of ureas (**T.9**-**T.17**) that lacked this structural fragment. These compounds have shown antiproliferative and apoptotic activity at lower doses than the triazolyl derivatives. In general, derivatives with *(E)* configuration in the stilbene subunit have been the most active ones improving the biological results obtained for the reference compounds. More specifically, **T.13** (*m*-Cl) and **T.14** (*p*-Cl) inhibit tube formation of endothelial cells at 0.1 μM and show inhibition of VEGFR-2 tyrosine kinase activity at lower concentrations than the triazolyl ureas and the reference compound BMS-8. As regards immunomodulator effect, they are able to improve the effect of BMS-8 in the inhibition of PD-L1 and c-Myc proteins. **T.14** has been the most active stilbene urea in inhibiting cell proliferation in co-cultures, with an increase in antiproliferative effect of more than 80%.

In summary, compounds **T.2** (triazole, *m*-Cl), **T.13** (*E*-stilbene, *m*-Cl) and **T.14** (*E*-stilbene, *p*-Cl) show the best antiangiogenic and immunomodulator properties for every group of synthetized compounds. This has let us to conclude that the presence of a chlorophenyl urea unit is important for the dual action of these kind of derivatives. Even so, a comparison of the results obtained for the triazolyl ureas with those achieved with the stilbene ureas has led us to conclude that the presence of the triazole ring in these aryl urea derivatives does not improve the biological activity when compared to the reference compounds. However, the substitution of the triazole ring for the *E*-stilbene unit leads to the enhancement of the expected dual biological activity. To the best of our knowledge,

this is the first example of the design and synthesis of compounds with both anti-PD-L1 and anti-angiogenic effect, so that a new door is opened to new kind of promising targeted anticancer agents.

4. Experimental

4.1. Docking studies

Molecular docking was performed using Autodock 4.2 [12]. The crystal structures of the VEGFR-2 kinase domain (PDB ID: 3EWH) and PD-L1 (PDB ID: 4ZQK) were used as templates. Ligands were previously removed from the protein structure in order to perform docking simulation. Discovery Studio Visualizer program [20] was used to build the structures of ureas **T.1-T.17**. The cluster was compared on the basis of the free energy of binding. The Lamarckian genetic algorithm (LGA) was employed with the default parameters; g_eval was set to 2500000 (medium) and 100 LGA runs were conducted. Molecular graphics were done with PYMOL (PyMOL Molecular Graphics System, version 1.6).

4.2. Chemistry

4.2.1. General procedures

NMR spectra were measured at 25°C. The signals of the deuterated solvent ($CDCl_3$ or DMSO) were taken as the reference. Multiplicity assignments of ^{13}C signals were made by means of the DEPT pulse sequence. Complete signal assignments in ^{1}H and ^{13}C NMR spectra were made with the aid of 2D homo- and heteronuclear pulse sequences (COSY, HSQC, HMBC). High resolution mass spectra were run by the electrospray mode (ESMS). IR data were measured with oily films on NaCl plates (oils) and are given only for relevant functional groups (C=O, NH). Experiments which required an inert atmosphere were carried out under dry N_2 in flame-dried glassware. Commercially available reagents were used as received.

4.2.2. Experimental procedure for the synthesis of 1-methoxy-4-(prop-2-yn-1-yl)benzene

(4-methoxyphenyl)methanol (1 eq) was dissolved in CH_2Cl_2 (1.5 mL/mmol) and cooled at 0ºC. Then, PBr_3 (1 eq) was slowly added and the mixture was stirred at 0ºC under inert atmosphere. After three hours, the mixture was poured over a saturated aqueous solution of $NaHCO_3$ and extracted with CH_2Cl_2. The organic solvent was evaporated under reduced pressure and the crude residue was purified by means of flash

silica gel chromatography (hexane) to afford 1-(bromomethyl)-4-methoxybenzene. The latter compound and CuCl (0.5 eq) were added to an ethynylmagnesium bromide (2 eq) solution 0.5 M in THF. The mixture was stirred at reflux (70ºC) for 2 h. The reaction mixture was then cooled and poured over a saturated aqueous solution of NH_4Cl, followed by extraction (3 times) with Et_2O. The organic phase was washed with H_2O and brine and dried over anhydrous $MgSO_4$. After evaporation of all volatiles under reduced pressure, the crude residue was purified by flash silica gel chromatography (hexane:EtOAc mixtures as eluent) to afford 1-methoxy-4-(prop-2-yn-1-yl)benzene as a yellowish oil (57%).

*4.2.3. Experimental procedure for the synthesis of azido-ureas **2-9**.*

A solution of 2-azidoethan-1-amine **1** (1 eq) in DMF was treated with Et_3N (2 eq). The solution was stirred for 10 min at rt and then CDI (2 eq) was added. The resulting mixture was stirred for 20 min at rt. Then, the corresponding aniline (2 eq) was added to the reaction mixture and this was stirred overnight at 50ºC. After this time, the solvent of the reaction mixture was evaporated under reduced pressure and the crude was purified by flash silica gel chromatography (hexane:EtOAc mixtures as eluent) to afford the desired products **2-9**.

*4.2.4. Experimental procedure for the synthesis of triazolyl-ureas **T.1**-**T.8**.*

A solution of 1-methoxy-4-(prop-2-yn-1-yl)benzene (1 eq) in DMF was treated with the corresponding previously prepared azido-ureas (1.2 eq). Then, a mixture of $CuSO_4 \cdot 5H_2O$ (0.1 eq) and sodium ascorbate (0.1 eq) in DMF/H_2O (9:1) was added to the reaction mixture which was stirred for 2 h at 60ºC. After that time, the mixture was concentrated, redissolved in EtOAc, and washed with brine repeated times. Finally, the organic solvent evaporated under reduced pressure and the crude was purified by flash silica gel (hexane:EtOAc mixtures as eluent) to afford the desired products. Detailed analytical data ate given in the Supplementary Material.

*4.2.5. Experimental procedure for the synthesis of phosphonium salt **11**.*

A solution of 3-nitrobenzyl bromide **D10** (4.63 mmol) and triphenylphosphine (4.63 mmol) in dry CH_2Cl_2 (20 mL) was stirred for 3 h at rt. After the reaction was complete,

the white precipitate was filtered and sequentially washed with CH_2Cl_2 and hexane affording **11** as a white solid (1.56 g, 71%, m. p. 273ºC).

4.2.6. Experimental procedure for Wittig reaction (Scheme 2, b).

4-methoxybenzaldehyde (3.26 mmol) was dissolved in CH_2Cl_2 (20 mL) and then, the phosphonium salt **11** (3.26 mmol), K_2CO_3 (3.6 mmol) and 18-crown-6 (0.6 mmol) were added to the solution. The mixture was refluxed overnight and then was filtered and concentrated affording 810 mg (73% yield) of compound **12** as an *E/Z* stereoisomeric mixture.

4.2.7. Experimental procedure for nitro group reduction (Scheme 2, c).

Zn (0.6 mol) was added to a solution of compound **12** (4.08 mmol) in AcOH (133 mL). The resulting mixture was vigorously stirred at rt for 1 h in a flask that was protected from the light. Then, the solids were filtered over Celite to remove the Zn, and were thoroughly washed with EtOAc. The filtrate was neutralized with saturated aqueous $NaHCO_3$ and the organic phase was separated and dried over $MgSO_4$ anhydride. After filtration and solvent evaporation, silica gel column chromatography (hexane-EtOAc mixtures as eluent) was used to isolate the stereoisomers **13** and **14** (*Z/E* 6:4).

4.2.8. Experimental procedure for hydrogenation (Scheme 2, d).

Compound **12** (2.35 mmol) was dissolved in EtOAc (30 ml) and stirred with 10 % Pd/C (300 mg) for 2 h at rt and ambient pressure under a hydrogen atmosphere. The resulting mixture was filtered through a pad of Celite and the filtrate was evaporated under reduced pressure. Then, the residue was purified by silica gel column chromatography (hexane-EtOAc mixtures as eluent) to give compound **15** as a brownish solid (66%, m. p. 81-85ºC).

*4.2.9. Experimental procedure for the synthesis of carbamates **16-18**.*

A solution of **13**, **14** or **15** (1 eq.) in THF (5 mL/mmol) was cooled at 0ºC and anhydrous pyridine (2.4 eq.) and phenyl chloroformate (1.4 eq.) was added under inert atmosphere. The resulting mixture was stirred in the dark for 20 min at 0ºC and then for 1 h at rt. After this time, H_2O (5 mL/mmol) and HCl 1 M (2.5 mL/mmol) were added to the reaction mixture, which was then extracted with CH_2Cl_2 (3 x 20 mL). The organic layer was washed with brine, and then dried on anhydrous Na_2SO_4. Removal of volatiles under reduced pressure afforded an oily residue which was subjected to column

chromatography on silica-gel (hexane-EtOAc mixtures as eluent) to yield the desired products **16**-**18**.

*4.2.10. Experimental procedure for the synthesis of ureas **T.9**-**T.17**.*

A solution of the corresponding chloroaniline (0.5 mmol) in dry THF (4 mL/mmol) was treated with Et_3N (5.4 mmol) under inert atmosphere. After stirring the mixture for 5 min, the corresponding previously prepared carbamate (0.5 mmol) was added dropwise as a solution in THF (10 mL/mmol). The resulting mixture was then stirred in the dark at 40-50 ºC for 24-72 h (TLC monitoring). After this time, CH_2Cl_2 (15 mL) and HCl 1M were added to the reaction mixture, which was then extracted with CH_2Cl_2 (2 x 10 mL). The organic layer was washed with brine and then dried on anhydrous Na_2SO_4. Removal of volatiles under reduced pressure afforded an oily residue which was subjected to column chromatography on silica-gel (hexane-EtOAc mixtures as eluent) to afford the desired products. Detailed analytical data ate given in the Supplementary Material.

4.3. Biological studies

4.3.1. Cell culture

Cell culture media were purchased from Gibco (Grand Island, NY). Fetal bovine serum (FBS) was obtained from Harlan-Seralab (Belton, U.K.). Supplements and other chemicals not listed in this section were obtained from Sigma Chemical Co. (St. Louis, MO). Plastics for cell culture were supplied by Thermo Scientific BioLite. All tested compounds were dissolved in DMSO at a concentration of 10 mM and stored at −20°C until use.

HT-29, MCF-7, HeLa, A549 and HEK-293 cell lines were maintained in Dulbecco's modified Eagle's medium (DMEM) containing glucose (1 g/L), glutamine (2 mM), penicillin (50 μg/mL), streptomycin (50 μg/mL), and amphotericin B (1.25 μg/mL), supplemented with 10% FBS. HMEC-1 cell line was maintained in Dulbecco's modified Eagle's medium (DMEM)/Low glucose containing glutamine (2 mM), penicillin (50 μg/mL), streptomycin (50 μg/mL), and amphotericin B (1.25 μg/mL), supplemented with 10% FBS. For the development of tube formation assays in Matrigel, HMEC-1 cells were cultured in EGM-2MV Medium supplemented with EGM-2MV SingleQuots.

4.3.2. Cell proliferation assay

In 96-well plates, 3×10^3 (HeLa, A549, HMEC-1, HEK-293) or 5×10^3 (HT-29, MCF-7) cells per well were incubated with serial dilutions of the tested compounds in a total volume of 100 μL of their respective growth media. The 3-(4,5-dimethylthiazol-2-yl)-2,5-diphenyltetrazolium bromide (MTT; Sigma Chemical Co.) dye reduction assay in 96-well microplates was used, as previously described [21]. After 2 days of incubation (37 °C, 5% CO_2 in a humid atmosphere), 10 μL of MTT (5 mg/mL in phosphate-buffered saline, PBS) was added to each well, and the plate was incubated for a further 3 h (37 °C). After that, the supernatant was discarded and replaced by 100 μL of DMSO to dissolve formazan crystals. The absorbance was then read at 540 nm by spectrophotometry. For all concentrations of compound, cell viability was expressed as the percentage of the ratio between the mean absorbance of treated cells and the mean absorbance of untreated cells. Three independent experiments were performed, and the IC_{50} values (i.e., concentration half inhibiting cell proliferation) were graphically determined using GraphPad Prism 4 software.

4.3.3. Apoptosis assay

Apoptosis was determined by quantifying FITC-Annexin V translocation by means of flow cytometry. A549 cells were incubated with compounds for 24 h and then stained following instructions of BD Apoptosis Detection™ Kit. Analysis was performed with a BD Accuri™ C6 flow cytometer.

4.3.4. VEGFR-2 quantification by flow cytometry

VEGFR-2 was determined quantifying Alexa Fluor® 647 Mouse Anti-Human CD309 (VEGFR-2) by means of flow cytometry. To detect membrane VEGFR-2, cells were incubated with compounds for 24 h and then they were collected, fixed and stained with Alexa Fluor® 647 Mouse Anti-Human CD309 (VEGFR-2). For the detection of total VEGFR-2 (membrane and cytosolic), cells were incubated with compounds for 24 h, then lysates were obtained and stained with Alexa Fluor® 647 Mouse Anti-Human CD309 (VEGFR-2).

4.3.5. Total VEGFR-2 determination by immunofluorescence

A549 cells were plated on cover glass and incubated with the different compounds for 24 h. Then, they were permeabilized with PEM-Triton-X-100 0.5% and fixed in 3.7% formaldehyde. Direct immunostaining was carried out for 2 h at 37°C in darkness with Alexa Fluor® 647 Mouse Anti-Human CD309 (VEGFR-2). Then, cells were washed in

PBS and cover glasses were mounted with 10 μL of Glycine/Glycerol buffer. Images were obtained by a confocal laser scanning microscope (CLSM) Leica SP5 with a Leica inverted microscope, equipped with a Plan-Apochromat 63x oil immersion objective (NA=1.4). Each image was recorded with the CLSM's spectral mode selecting specific domains of the emission spectrum. Alexa Fluor®647 fluorophore was excited at 650 nm with an argon laser and its fluorescence emission was collected at 665 nm.

4.3.6. phospho-VEGFR-2 quantification by ELISA

For endothelial cells (HMEC-1): 5 x·10^5 cells/well were seeded in 6-well plates and once they were at 80% of their confluency, they were starved with medium containing 0.1% of FBS for 24 h. Then, cells were incubated with the corresponding compounds for 24 h and next cells were stimulated with 100 ng/ml of Recombinant VEGF-165 for 30 min at 37ºC. After that, lysates were collected, protein quantification was carried out by Bradford test and, then, and phospho-VEGFR-2 was quantified using PathScan® Phospho-VEGFR-2(Tyr1175) Sandwich ELISA Kit according to the manufacturer's instructions. **For tumor cells (A549):** 3·x 10^5 cells/well were seeded in 6-well plates and were incubated with the corresponding compounds at 10 μM for 24 h. After that, lysates were collected, protein quantification was carried out by Bradford test and, then, phospho-VEGFR-2 was quantified using PathScan® Phospho-VEGFR-2(Tyr1175) Sandwich ELISA Kit according to the manufacturer's instructions.

4.3.7. p-Erk quantification by western blot assay

From the lysates extracted in the previous experiment (5.3.6), 100 μg of proteins were subjected to gel electrophoresis using Bolt 4-12% Bis-Tris plus gels. Then, proteins were transferred to Hybond-P polyvinylidene difluoride (PVDF) membranes using the iBlot gel transfer system, and the resulting membranes were incubated first for 1 h at rt in blocking buffer (5% non-fat dry milk in TBS 1x containing 0.1% Tween) and subsequently overnight at 4 ºC in TBST buffer primary antibody solution (Anti-ERK1+ERK2 phosphoT202+T204). After washing, membranes were incubated with the corresponding HRP-conjugated secondary antibody in blocking buffer for 1 h at rt. Next, membranes were washed extensively and immunoreactive proteins were detected by chemiluminescence (ImageQuant LAS500).

4.3.8. Tube formation inhibition assay

Wells of a 96-well μ-plate for angiogenesis were coated with 12 μL of Matrigel® (10 mg/mL, BD Biosciences) at 4ºC. After gelatinization at 37ºC for 30 min, HMEC-1 cells were seeded at 2 x 10^4 cells/well in 35 μL of culture medium on top of the Matrigel and were incubated 30 min at 37ºC while are attached. Then, compounds were added dissolved in 35 μL of culture medium and after 20 h of incubation at 37ºC, tube destruction was evaluated.

4.3.9. PD-L1 and c-Myc quantification by ELISA

A549 cells were seeded ($3 \cdot 10^5$ cells/well) in 6-well plates and were incubated with the corresponding compounds for 24 h. After that, lysates were collected, protein quantification was carried out by Bradford test and, then, PD-L1 and c-Myc were quantified using Human PD-L1 ELISA Kit 28-8 (ab214565) and c-Myc (Total) Human ELISA Kit (KHO2041), respectively, according to the manufacturer's instructions.

4.3.10. PD-L1 and c-Myc determination by immunofluorescence

A549 cells were plated on cover glass and incubated with the different compounds for 24 h. Then, they were permeabilized with PEM-Triton-X-100 0.5% and fixed in 3.7% formaldehyde. Direct immunostaining was carried out for 2 h at 37°C in darkness with Anti-PD-L1-AlexaFluor®647 and Anti-c-Myc-FITC. Then, cells were washed in PBS and cover glasses were mounted with 10 μL of Glycine/Glycerol buffer. Images were obtained by a confocal laser scanning microscope (CLSM) Leica SP5 with a Leica inverted microscope, equipped with a Plan-Apochromat 63x oil immersion objective (NA=1.4). Each image was recorded with the CLSM's spectral mode selecting specific domains of the emission spectrum. Alexa Fluor®647 fluorophore was excited at 650 nm with an argon laser and its fluorescence emission was collected at 665 nm. FITC fluorophore was excited at 488 nm with an argon laser and its fluorescence emission was collected between 496 nm and 535 nm.

4.3.11. Cell proliferation evaluation in co-cultures

In 6-well plates, 5 x 10^4 tumor cells per well were seeded and incubated for 24 h with the tested compounds at 200 μM in a total volume of 1.5 mL in the presence of 2×10^5 Jurkat T cells per well. Then, supernatant was discarded, tumor cells were collected with trypsin and counted using the Neubauer chamber.

Acknowledgements

This research has been funded by the Ministerio de Economía y Competitividad (project CTQ2014-52949-P) and by the Universitat Jaume I (projects PI-1B2015-75 and UJI-B2018-38). L. C-M. thanks the Spanish Ministry of Education, Culture and Sport for an FPU fellowship (FPU14/00878). The authors are also grateful to the SCIC of the Universitat Jaume I for providing NMR and Mass Spectrometry facilities.

Supplementary Information

Analytical and graphical spectroscopic data of all new synthetic compounds are provided in the Supplementary Information.

References

[1] P. Gotwals, S. Cameron, D. Cipolletta, V. Cremasco, A. Crystal, B. Hewes, B. Mueller, S. Quarantino, C. Sabatos-Peyton, L. Petruzzelli, J. A. Engelman, G. Dranoff. Prospects for combining targeted and conventional cancer therapy with immunotherapy, *Nat. Rev. Cancer* **2017**, *17*, 286-301.

[2] G. Bergers, L. E. Benjamin. Tumorigenesis and the angiogenic switch, *Nat. Rev. Cancer* **2003**, *3*, 401-410.

[3] K. Holmes, O. L. Roberts, A. M. Thomas, M. J. Cross. Vascular endothelial growth factor receptor-2: structure, function, intracellular signalling and therapeutic inhibition, *Cell. Signal.* **2007**, *19*, 2003-2012.

[4] H. O. Alsaab, S. Sau, R. Alzhrani, K. Tatiparti, K. Bhise, S. K. Kashaw, A. K. Iyer. PD-1 and PD-L1 checkpoint signaling inhibition for cancer immunotherapy: mechanism, combinations and clinical outcome, *Front. Pharmacol.* **2017**, *8*, 561.

[5] L. Skalniak, K. M. Zak, K. Guzik, K. Magiera, B. Musielak, M. Pachota, B. Szelarek, J. Kocik, P. Grudnik, M. Tomala, S. Krzanik, K. Pyrc, A. Dömling, G. Dubin, T. A. Holak. Small-molecule inhibitors of PD-1/PD-L1 immune checkpoint alleviate the PD-L1-induced exhaustion of T-cells, *Oncotarget* **2017**, *8*, 72167-72181.

[6] S. C. Casey, L. Tong, Y. Li, R. Do, S. Walz, K. N. Fitzgerald, A. M. Gouw, V. Baylot, I. Gütgemann, M. Eilers, D. W. Felsher. MYC regulates the antitumor immune response through CD47 and PD-L1, *Science* **2016**, *352*, 227-231.

[7] S. C. Casey, V. Baylot, D. W. Felsher, MYC: Master regulator of immune privilege, *Trends Immunol.* **2017**, *38*, 298-305.

[8] M. McTigue, B. W. Murray, J. H. Chen, Y. L. Deng, J. Solowiej, R. S. Kania, Molecular conformations, interactions and properties associated with drug efficiency and

clinical performance among VEGFR TK inhibitors, *Proc. Natl. Acad. Sci. USA* **2012**, *109*, 18281-18289.

[9] (a) F. Meng, Molecular dynamics simulation of VEGFR2 with sorafenib and other urea-substituted aryloxy compounds, *Journal of Theoretical Chemistry* **2013**, http://dx.doi.org/10.1155/2013/739574. (b) T. Wei, W. Tu, B. Zhao, Y. Lan, J. Bao, Z. Dai, Monitoring of an important biomarker and target protein: VEGFR2 in cell lysates, *Sci. Rep.* **2014**, *4*, 3982.

[10] L. S. Chupak, X. Zheng, Compounds useful as immunomodulators, PCT Int. Appl. (2015), WO 2015034820 A1 20150312.

[11] (a) K. M. Zak, P. Grudnik, K. Guzik, B. J. Zieba, B. Musielak, A. Dömling, G. Dubin, T. A. Holak. Structural basis for small molecule targeting of the programmed death ligand 1 (PD-L1), *Oncotarget* **2016**, *7*, 30323-30335. (b) K. Guzik, K. M. Zak, P. Grudnik, K. Magiera, B. Musielak, R. Törner, L. Skalniak, A. Dömling, G. Dubin, T. A. Holak, Small-molecule inhibitors of the programmed cell death-1/programmed death-ligand 1 (PD-1/PD-L1) interaction via transiently induced protein states and dimerization of PD-L1, *J. Med. Chem.* **2017**, *60*, 5857-5867.

[12] G. M. Morris, R. Huey, W. Lindstrom, M. F. Sanner, R. K. Belew, D. S. Goodsell, A. J. Olson, AutoDock4 and AutoDockTools4: Automated docking with selective receptor flexibility, *J. Comput. Chem.* **2009**, *30*, 2785-2791.

[13] Aminoazide **1** was prepared according to S. Loison, M. Cottet, H. Orcel, H. Adihou, R. Rahmeh, L. Lamarque, E. Trinquet, E. Kellenberger, M. Hibert, T. Durroux, B. Mouillac, Bonnet, D. Selective Fluorescent Nonpeptidic Antagonists For Vasopressin V_2 GPCR: Application To Ligand Screening and Oligomerization Assays, *J. Med. Chem*. **2012**, *55*, 8588-8602.

[14] V. V. Rostovtsev, L. G. Green, V. V. Fokin, K. B. Sharpless, A Stepwise Huisgen Cycloaddition Process: Copper(I)-Catalyzed Regioselective “Ligation” of Azides and Terminal Alkynes, *Angew. Chem. Int. Ed.* **2002**, *41*, 2596-2599.

[15] S. G. Almalki, D. K. Agrawal, ERK signaling is required for VEGF-A/ VEGFR2-induced differentiation of porcine adipose-derived mesenchymal stem cells into endothelial cells, *Stem Cell Res. Ther.* **2017**, *8*, 113.

[16] S. P. Patel, R. Kurzrock, PD-L1 expression as a predictive biomarker in cancer immunotherapy, *Mol. Cancer Ther*. **2015**, *14*, 847-856.

[17] L. Conesa-Milián, E. Falomir, J. Murga, M. Carda, E. Meyen, S. Liekens, J. A. Marco, Synthesis and biological evaluation of carbamates derived from aminocombretastatin A-4 as vascular disrupting agents, *Eur. J. Med. Chem*. **2018**, *147*, 183-193.

[18] W. Sellers, D. E. Fisher, Apoptosis and cancer drug targeting, *J. Clin. Invest*. **1999**, *104*, 1655-1661.

[19] G. Pistritto, D. Trisciuoglio, C. Ceci, A. Garufi, G. D'Orazi, Apoptosis as anticancer mechanism: function and dysfunction of its modulators and targeted therapeutic strategies, *Aging* **2016**, *8*, 603-619.

[20] Dassault Systèmes BIOVIA, Discovery Studio Visualizer, v16.1.0.15350, San Diego: Dassault Systèmes, 2015.

[21] S. Rodríguez-Nieto, M. A. Medina, A. R. Quesada, A re-evaluation of fumagillin selectivity towards endothelial cells, *Anticancer Res.* **2001**, *21*, 3457-3460.

List of captions

Figure 1. Structure of sorafenib and non-peptidic inhibitors of PD-L1.

Figure 2. Identified general structures able to interact with the kinase domain of VEGFR-2 and PD-L1. The hydrogen bonds that can be formed with VEGFR-2 are indicated in red. The zones of the molecules that interact with the hydrophobic pockets of both binding sites are also indicated.

Figure 3. A) Superposition of **D.1** (orange), **D.2** (light blue), **D.3** (green) and sorafenib (grey) in the kinase domain of VEGFR-2. B). Superposition of **D.1** (orange), **D.2** (light blue), **D.3** (green) and BMS-202 (violet) at the PD-L1 binding site.

Figure 4. Potential multitarget inhibitors of VEFGR-2 and PD-L1.

Scheme 1

Table 1. Effect on VEGFR-2 in HMEC-1 cells.

Table 2. Effect on VEGFR-2 in A549 cells.

Table 3. p-VEGFR-2 and p-Erk1/2 detected in HMEC-1 cells.

Figure 5. Representative Western blot of p-Erk1/2 detection in HMEC-1 cells. β-actin was used as internal control.

Table 4. p-VEGFR-2 and p-Erk1/2 detected in A549 cells.

Figure 6. Representative Western blot of p-Erk1/2 detection in A549 cells. β-actin was used as internal control.

Table 5. Inhibition effect of tube formation.

Table 6. PD-L1 and c-Myc detection in A549 cells.

Figure 7. Inhibition of cell proliferation (%) in presence of Jurkat T cells. Data are representative of three experiments.

Scheme 2

Table 7. IC_{50} values (μM) for sunitinib, sorafenib, BMS-8 and derivatives **T.9-T.17**.

Figure 8. Apoptotic effect (%) in A549 cells. Data are representative of three experiments.

Table 8. Effect on VEGFR-2 expression in A549 cells.

Figure 9. Effect on VEGFR-2 expression in A549 cells (A) DMSO, (B) **T.13** and (C) **T.14**.

Table 9. Effect on VEGFR-2 expression in HMEC-1 cells.

Table 10. p-VEGFR-2 and p-Erk1/2 detected in A549 cells.

Figure 10. Representative Western blot of p-Erk1/2 detection in A549 cells. β-actin was used as internal control.

Table 11. Inhibition effect of tube formation.

Figure 11. Effect of **T.14** at 1, 0.1 and 0.01 μM concentrations (from left to right).

Table 12. PD-L1 and c-Myc proteins detection in A549 cells.

Figure 12. Effect on PD-L1 (red) and c-Myc (green) in A549 cells. (A) DMSO, (B) BMS-8, (C) **T.14**.

Figure 13. Inhibition of cell proliferation (%) in presence of Jurkat T cells. Data are representative of three experiments.

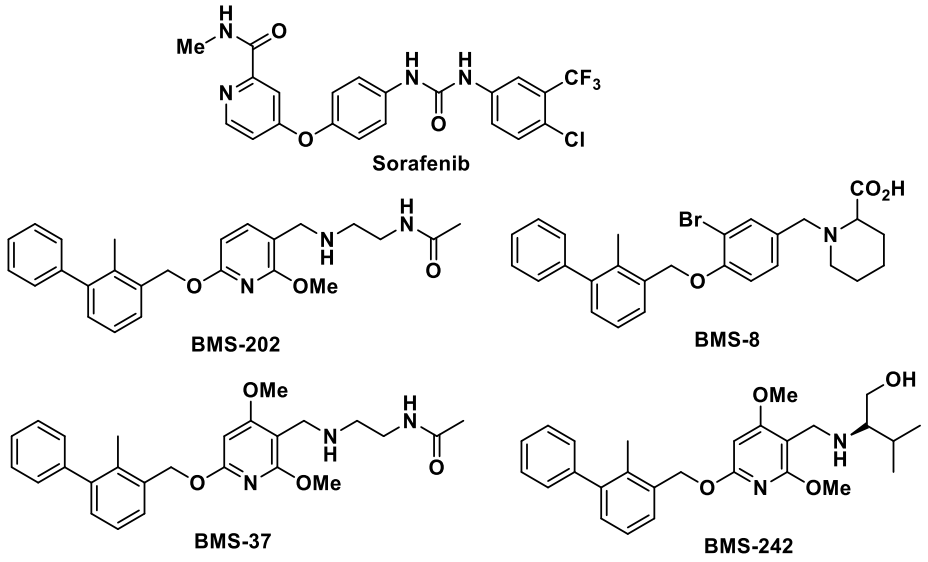

Figure 1

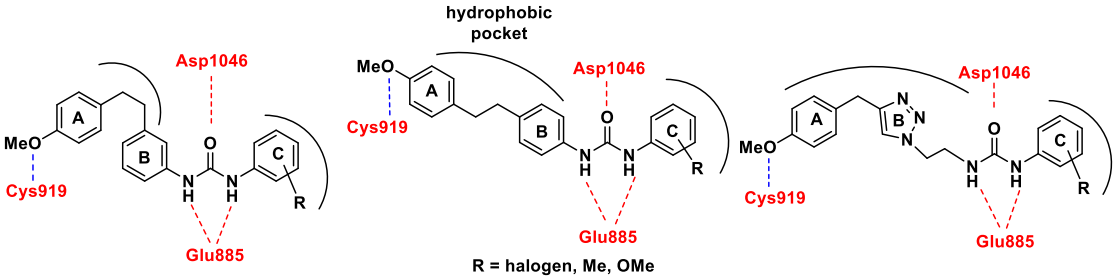
hydrophobic
pocket
Asp1046
MeO
Cys919
A
B
C
R
Glu885
R = halogen, Me, OMe

Figure 2

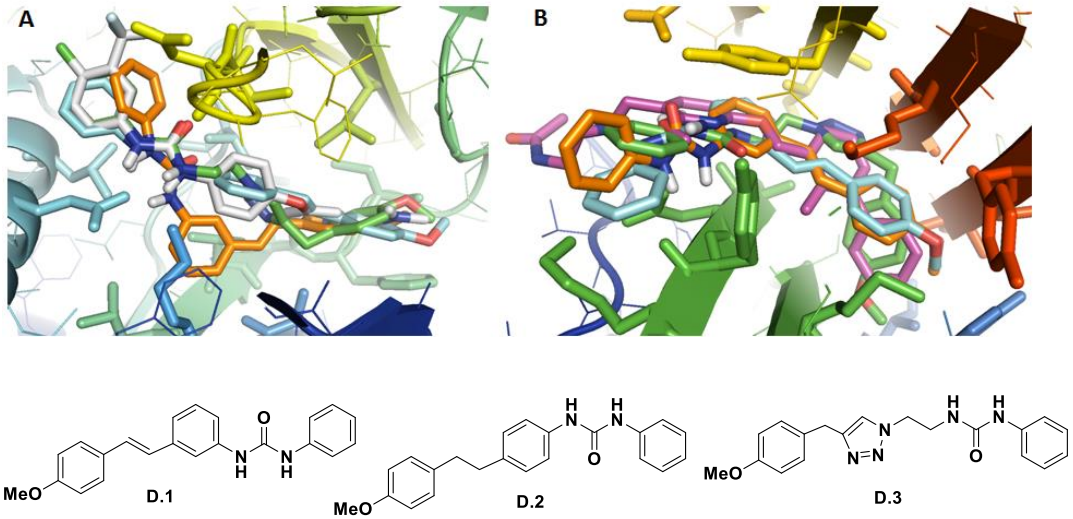

Figure 3

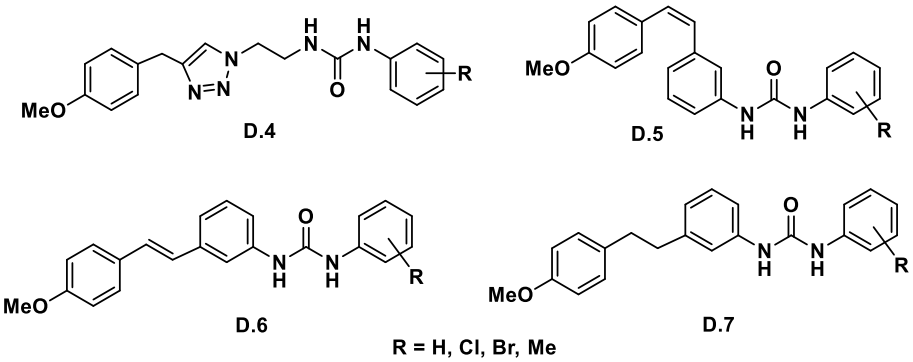

Figure 4

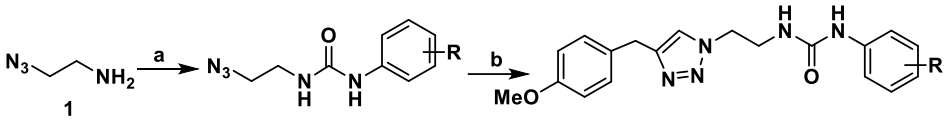

1

2 (R = H)
3 (R = *m*-Cl)
4 (R = *p*-Cl)
5 (R = *m*-Br)
6 (R = *p*-Br)
7 (R = *o*-Me)
8 (R = *m*-Me)
9 (R = *p*-Me)

T.1 (R = H)
T.2 (R = *m*-Cl)
T.3 (R = *p*-Cl)
T.4 (R = *m*-Br)
T.5 (R = *p*-Br)
T.6 (R = *o*-Me)
T.7 (R = *m*-Me)
T.8 (R = *p*-Me)

Scheme 1

Table 1

Comp.	Membrane VEGFR-2 (%)	Total VEGFR-2 (%)
Sorafenib	46 ± 8	64 ± 4
T.1	97 ± 14	105 ± 10
T.2	74 ± 6	81 ± 14
T.3	90 ± 4	102 ± 5
T.4	79 ± 10	78 ± 1
T.5	40 ± 10	55 ± 5
T.6	79 ± 9	100 ± 11
T.7	76 ± 4	91 ± 9
T.8	97 ± 15	90 ± 7

Data are the average (±SD) of three experiments.

Table 2

Comp.	Membrane VEGFR-2 (%)	Total VEGFR-2 (%)
Sorafenib	92 ± 3	85 ± 5
Sunitinib	66 ± 8	135 ± 14
T.2	95 ± 3	86 ± 6
T.4	98 ± 6	80 ± 8
T.5	70 ± 4	61 ± 11

Data are the average (±SD) of three experiments.

Table 3

Comp.	HMEC-1 p-VEGFR-2 (%)	HMEC-1 p-Erk1/2 (%)
Sorafenib	77 ± 9	80 ± 8
T.1	100 ± 12	-
T.2	70 ± 16	38 ± 14
T.3	86 ± 3	72 ± 6
T.4	>100	-
T.5	>100	-
T.6	83 ± 4	82 ± 11
T.7	90 ± 10	-
T.8	>100	-

Data are the average (±SD) of three experiments.

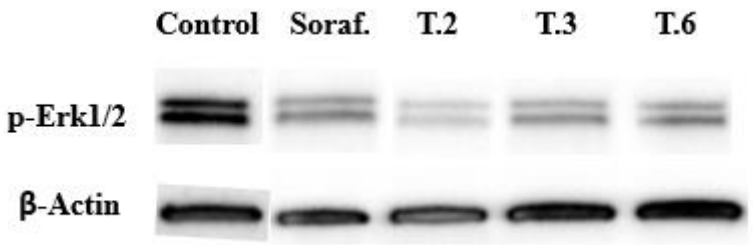

Figure 5

Table 4

Comp.	A549 p-VEGFR-2 (%)	A549 p-Erk1/2 (%)
Sorafenib	84 ± 4	50 ± 7
T.2	121 ± 11	99 ± 9
T.3	125 ± 12	78 ± 7
T.6	121 ± 16	119 ± 8
T.7	112 ± 10	90 ± 13

Data are the average (±SD) of three experiments.

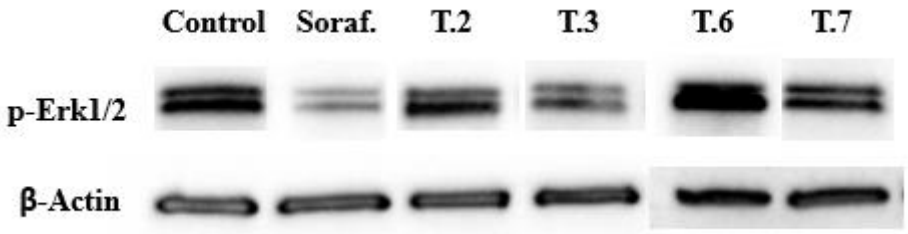

Figure 6

Table 5

Comp.	Minimum active conc. (µM)
Sunitinib	3
Sorafenib	10
T.2	50
T.3	400
T.6	200

Data are representative of three experiments.

Table 6

Comp.	% PD-L1	% c-Myc
BMS-8	68 ± 5	60 ± 7
T.1	83 ± 9	-
T.2	70 ± 8	60 ± 8
T.3	69 ± 10	73 ± 5
T.4	80 ± 12	-
T.5	>100	-
T.6	82 ± 20	-
T.7	90 ± 20	-
T.8	66 ± 6	70 ± 8

Data are the average (±SD) of three experiments.

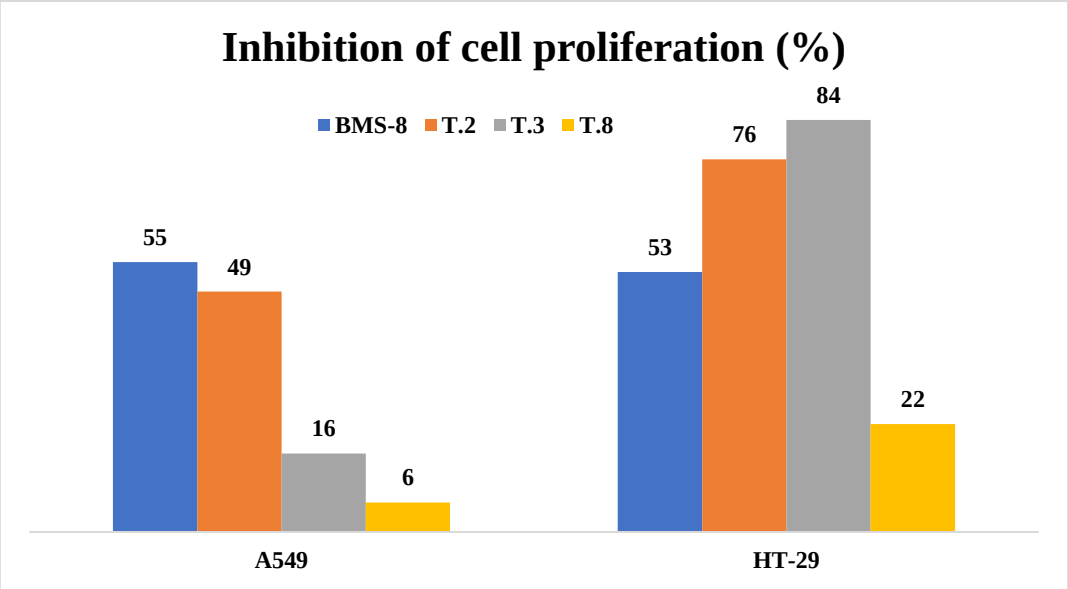
Inhibition of cell proliferation (%)
BMS-8
T.2
T.3
T.8
55
49
16
6
53
76
84
22
A549
HT-29

Figure 7

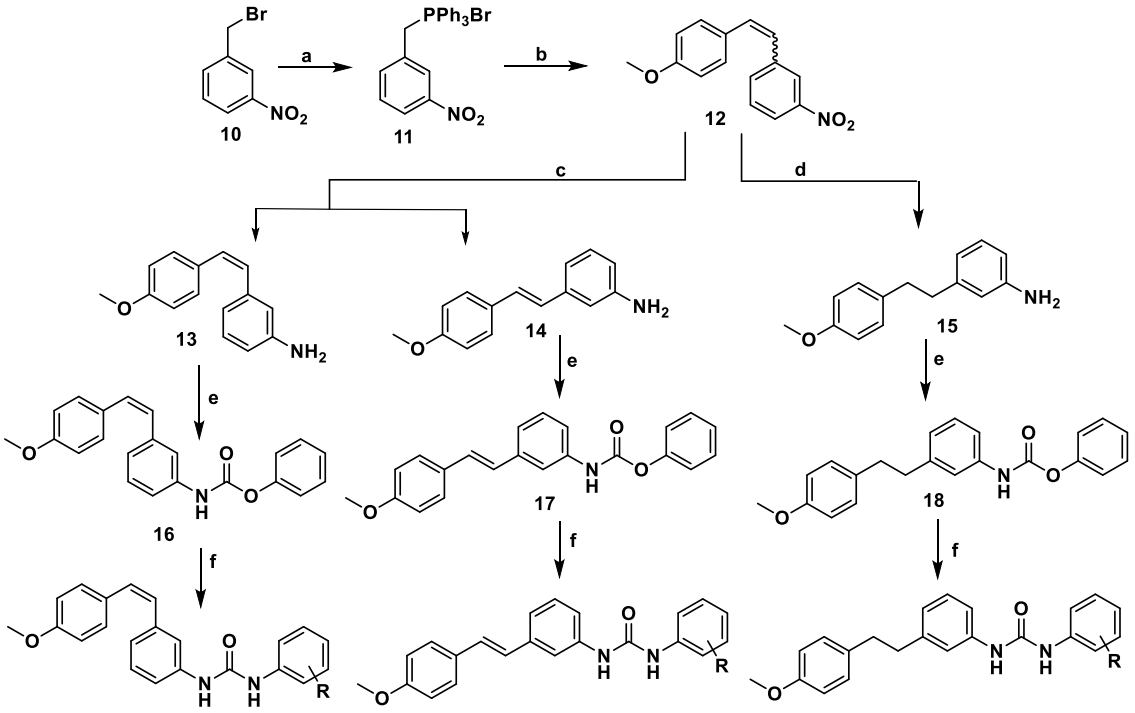
Br
a
PPh3Br
b
NO2
10
11
12
c
d
13
14
15
NH2
e
16
17
18
f
R
T.9 (R = o-Cl)
T.10 (R = m-Cl)
T.11 (R = p-Cl)
T.12 (R = o-Cl)
T.13 (R = m-Cl)
T.14 (R = p-Cl)
T.15 (R = o-Cl)
T.16 (R = m-Cl)
T.17 (R = p-Cl)

Scheme 2

Table 7

Comp.	HT-29	MCF-7	HeLa	A549	HMEC-1	HEK-293
Sunitinib	3.8 ± 0.5	0.08 ± 0.02	7.8 ± 1.0	11 ± 2	7 ± 4	5.0 ± 0.8
Sorafenib	17 ± 4	14 ± 4	6.1 ± 0.4	27 ± 2	34 ± 3	5.0 ± 0.7
BMS-8	19 ± 2	20 ± 3	>100	6 ± 1	-	60 ± 10
T.9	12 ± 4	19 ± 2	22 ± 3	21 ± 9	33.0 ± 0.6	6.5 ± 0.2
T.10	20 ± 10	37.2 ± 0.8	10.5 ± 0.6	38 ± 3	32.9 ± 0.5	5 ± 2
T.11	33 ± 5	17 ± 3	8 ± 1	29 ± 3	33 ± 3	20 ± 10
T.12	47 ± 4	>100	>100	61 ± 3	>100	57 ± 3
T.13	3.5 ± 0.6	4.3 ± 0.7	11.3 ± 0.7	7.7 ± 0.2	2 ± 1	2.4 ± 0.6
T.14	0.52 ± 0.09	0.40 ± 0.09	0.7 ± 0.3	1.5 ± 0.9	1.8 ± 0.8	1.0 ± 0.4
T.15	20 ± 3	>100	69 ± 5	24 ± 5	48 ± 7	90 ± 10
T.16	14 ± 4	8.2 ± 0.6	16.5 ± 0.7	>200	50 ± 20	5.3 ± 0.9
T.17	1.5 ± 0.1	15.3 ± 0.4	21 ± 1	>200	>200	1.8 ± 0.7

IC_{50} values are expressed as the compound concentration that inhibits the cell growth by 50%. Data are the average (±SD) of three experiments.

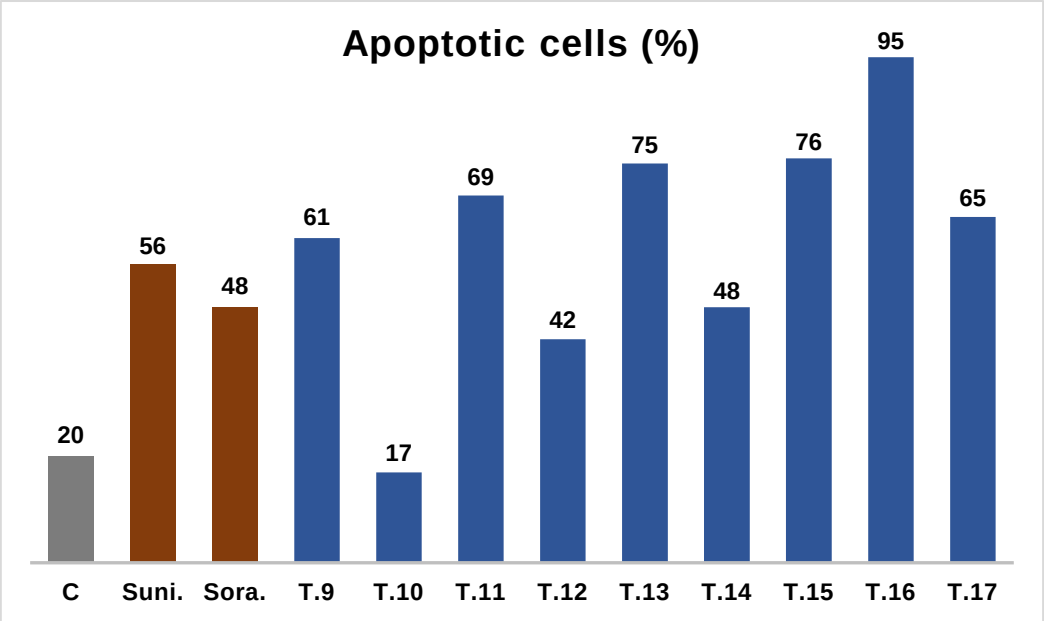
Apoptotic cells (%)
20
56
48
61
17
69
42
75
48
76
95
65
C
Suni.
Sora.
T.9
T.10
T.11
T.12
T.13
T.14
T.15
T.16
T.17

Figure 8

Table 8

Comp.	Membrane VEGFR-2 (%)	Total VEGFR-2 (%)
Sorafenib	92 ± 3	85 ± 5
Sunitinib	66 ± 8	135 ± 14
T.9	114 ± 20	177 ± 9
T.10	102 ± 10	186 ± 10
T.11	118 ± 3	100 ± 7
T.12	109 ± 18	42 ± 9
T.13	52 ± 10	32 ± 4
T.14	56 ± 11	10 ± 2
T.15	100 ± 19	100 ± 16
T.16	97 ± 10	98 ± 3
T.17	97 ± 11	96 ± 7

Data are the average (±SD) of three experiments.

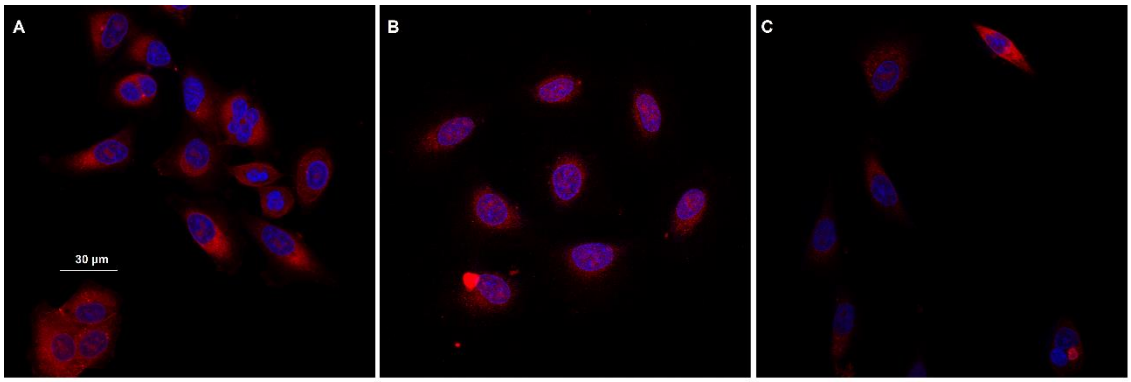

Figure 9

Table 9

Comp.	Membrane VEGFR-2 (%)	Total VEGFR-2 (%)
Sorafenib	46 ± 8	64 ± 4
T.12	76 ± 9	121 ± 8
T.13	55 ± 8	106 ± 16
T.14	56 ± 8	109 ± 17

Data are the average (±SD) of three experiments.

Table 10

Comp.	A549 p-VEGFR-2 (%)	A549 p-Erk1/2 (%)
Sorafenib	84 ± 4	50 ± 7
T.12	76 ± 3	100 ± 18
T.13	75 ± 5	56 ± 12
T.14	82 ± 3	66 ± 8

Data are the average (±SD) of three experiments.

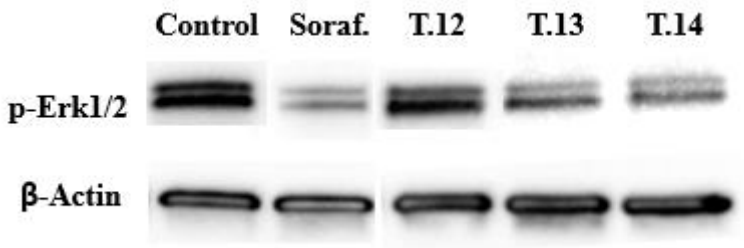

Figure 10

Table 11

Comp.	Minimum active conc. (µM)
Sunitinib	3
Sorafenib	10
T.9	10
T.10	10
T.11	1
T.12	10
T.13	0.1
T.14	0.1
T.15	1
T.16	10
T.17	100

Data are representative of three experiments.

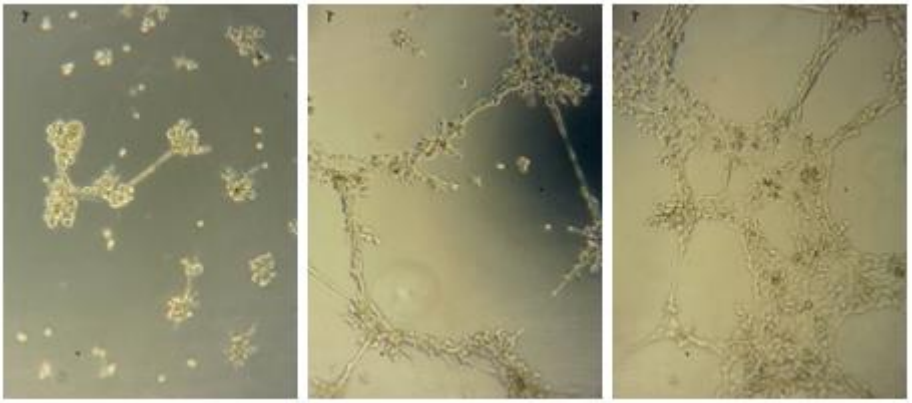

Figure 11

Table 12

Comp.[a]	% PD-L1	% c-Myc
BMS-8	68 ± 5	60 ± 7
T.9	83 ± 3	-
T.10	92 ± 10	-
T.11	75 ± 6	-
T.12	74 ± 7	-
T.13	49 ± 8	65 ± 12
T.14	25 ± 9	37 ± 5
T.15	61 ± 6	63 ± 11
T.16	51 ± 9	51 ± 10
T.17	38 ± 3	44 ± 6

[a] **T.9**-**T.14** were tested at 15 μM. BMS-8 and **T.15**-**T.17** were tested at 100 μM. Data are the average (±SD) of three experiments.

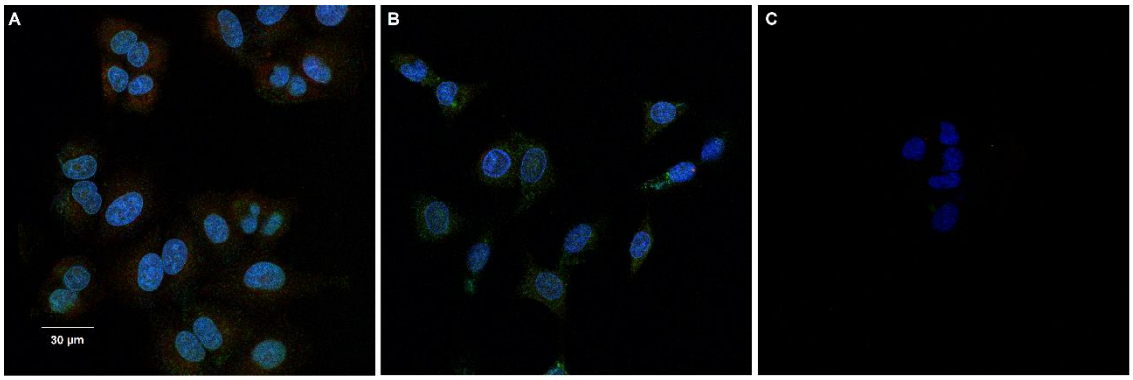

Figure 12

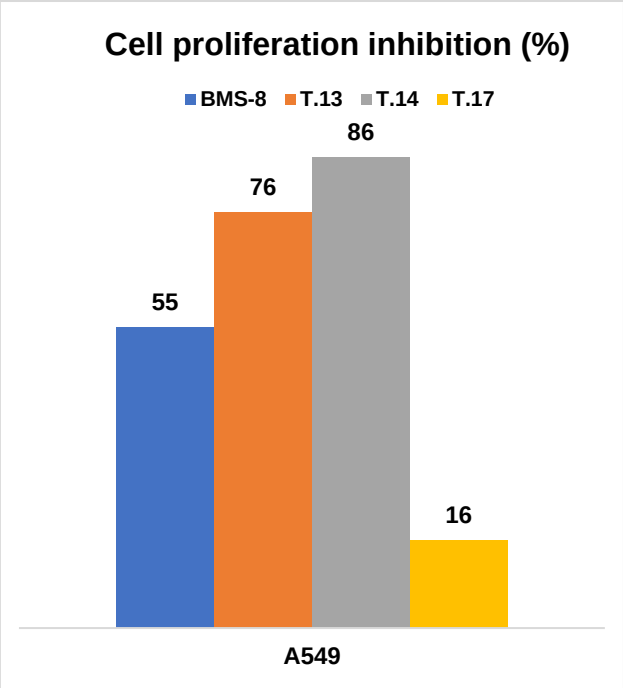
Cell proliferation inhibition (%)
BMS-8
T.13
T.14
T.17
55
76
86
16
A549

Figure 13